technische universität
dortmund

Thesis to obtain the academic degree
Master of Science

Floquet behavior for lattice fermions driven by light

Mona H. Kalthoff
born in Wuppertal

2018

Lehrstuhl für Theoretische Physik I
Fakultät Physik
Technische Universität Dortmund

Department of Physics
Georgetown University
Washington, D.C.

First corrector:	Prof. Dr. Götz S. Uhrig
Second corrector:	Prof. Dr. James K. Freericks
Submission date:	September 24th, 2018

Abstract

Among the abundance of scenarios to drive systems out of equilibrium the Floquet regime of quasi-stationary Floquet states resulting from periodic driving is very appealing. It suggests that physical systems can be tailored by controlling external driving fields. But as many-body Floquet theory becomes more popular, it is important to find ways to connect theory with experiment. Theoretical calculations can have a periodic driving field that is always on, but experiment cannot. Hence, we need to know how long a driving field is needed before the system starts to look like the periodically driven Floquet system. We answer this question here for noninteracting band electrons in the infinite-dimensional limit by studying the properties of the system under pulsed driving fields and illustrating how they approach the Floquet limit. Thereby we determine the minimal pulse lengths needed to recover the qualitative and semiquantitative Floquet theory results.

In the second part of this thesis, we change from periodically driven noninteracting systems to interacting systems and derive the general spectral representation of retarded Green functions in the Floquet regime, thereby generalizing the well-known Lehmann representation from equilibrium many-body physics. The derived spectral Floquet representation allows us to prove the nonnegativity of spectral densities and to determine exact spectral sum rules, which can be employed to benchmark the accuracy of approximations to the exact Floquet many-body Green functions.

Kurzfassung

Unter der Vielzahl von Möglichkeiten Systeme aus dem Gleichgewicht zu treiben, ist das Floquet-Regime von quasi-stationären Floquet-Zuständen besonders attraktiv, da es erlaubt physikalische Systeme durch steuernde, externe Felder maßzuschneidern. Doch mit der steigenden Popularität der Vielteilchen-Floquet-Theorie wird es zunehmend wichtig, Möglichkeiten zu finden, die experimentellen Ergebnisse mit der Theorie in Einklang zu bringen. Theoretische Rechnungen können von treibenden Feldern ausgehen, die über eine unendliche Zeitspanne eingeschaltet sind, doch im Experiment sind diese Felder nicht realisierbar. Deshalb ist es notwendig heraus zu finden wie lange ein System getrieben werden muss, bevor es sich dem periodisch getriebenen Floquet System angleicht. Wir beantworten diese Frage für nicht-wechselwirkende Bandelektronen im unendlichdimensionalen Raum, indem wir die Eigenschaften von Systemen, welche an gepulste, treibende Felder koppeln, analysieren und zeigen, wie sie sich dem Floquet-Limes annähren. Auf diese Weise ermitteln wie die minimalen Pulslängen, die notwendig sind, um die qualitativen und semi-quantitativen Ergebnisse der Floquet Theorie zu reproduzieren.

Im zweiten Teil dieser Masterarbeit wechseln wir von nicht-wechselwirkenden zu wechselwirkenden Systemen und leiten die allgemeine Spektralfunktion von retardierten Greenfunktionen im Floquet-Regime her. So verallgemeinern wir die bekannte Lehmann-Darstellung aus der Gleichgewichts-Vielteilchenphysik auf periodisch getriebene Systeme. Die hergeleitete Spektralfunktion in Floquet Darstellung erlaubt es uns außerdem, die Nichtnegativität von Spektraldichten zu beweisen und exakte Summenregeln zu bestimmen,welche erlauben, die

Genauigkeit von Approximationen für Floquet-Vielteilchen-Greenfunktionen zu beurteilen und so auch zu verbessern.

List of Publications

Parts of this thesis have been published in:

1. M. H. Kalthoff, G. S. Uhrig, and J. K. Freericks
   "Emergence of Floquet behavior for lattice fermions driven by light pulses"
   Physical Review B **98**, 035138 (2018)
   DOI: `10.1103/PhysRevB.98.035138`

2. G. S. Uhrig, M. H. Kalthoff and J. K. Freericks
   "Positivity of the spectral densities of retarded Floquet Green functions"
   Preprint: `arxiv.org/abs/1808.10199` (2018)

Those papers were written in the course of my master studies and contain the major results presented in this thesis.

Contents

1 Introduction **1**

2 Methods **3**
2.1 Green functions 3
2.2 Floquet theory 6

3 Noninteracting lattice fermions driven by light pulses **9**
3.1 Model 10
3.2 Infinite sinusoidal driving 13
3.3 Semi-infinite sinusoidal driving starting at $t_0 = 0$ 16
3.4 Sinusoidal steplike pulse 19
3.5 Sinusoidal Gaussian pulse 21

4 Periodically driven, interacting systems **27**
4.1 Positivity of the spectral densities of retarded Floquet Green functions . . . 27
4.2 Dyson equation for periodically driven systems 34

5 Summary and outlook **38**

A Convolution of periodic functions **40**

B Sum rules for higher moments of the spectral densities in the Hubbard model **42**

Bibliography **44**

1 Introduction

Nonequilibrium many-body physics is a vibrant field, both from the experimental and from the theoretical side. Largely, this has been triggered by the ease with which one can tune and manipulate the time dependence of systems of ultracold atoms in optical lattices [1, 2]. But there also have been significant advances in solid state systems, which employ ultrafast pump-probe techniques to study electrons on femto-second timescales [3–5].

Periodically driven many-body systems are simpler than general nonequilibrium systems, because the Hamiltonian repetitively cycles through the same functional form again and again. Conceptually, Floquet theory for periodic linear differential equations (and also periodic Hamiltonians) [6–8] is a powerful tool to treat these periodically modulated quantum systems. Recently, it has become a topic of wide interest in the condensed-matter community, especially with the relationship between periodic driving and topological properties [9, 10]. A fundamental development is the notion of Floquet design, i.e., the possibility to engineer quantum systems with certain desired properties, e.g., with topological phases [9], by properly selecting the external drive, see, e.g., Refs. [11–14]. Floquet systems require the driving field to be present for all times. This presents a challenge experimentally, since the field must be turned on and then off in realistic experiments. In addition, it is expected that interacting Floquet systems which have been turned on for a long time will generally have runaway heating, and end up in the infinite-temperature limit. This motivates the question, how long does a pulsed field need to be in order to describe the Floquet regime well? We answer this question for noninteracting band electrons in chapter 3.

Experimentally, this is an important issue. Seminal work by the Gedik group showed how one can transiently change the topology of a topological insulator when driven by circularly polarized light [15]. Theory indicated how one can determine the bandgaps that opened [16]. But the theoretical premise of this work was that when we examine properties at the center of the pump pulse, they will look like the infinitely driven Floquet system. While this cannot be precisely true, it is approximately true. In this thesis, we examine this question in detail and determine criteria for which one can approximate the Floquet regime well, and we also show how one can average transient results to recover Floquet behavior in cases where the Floquet limit does not immediately emerge. We anticipate that much of these criteria for pulsed systems will continue to hold when interactions are added, but provide no proof of that conjecture.

Some previous theory has examined these pulsed systems in the transient regime. One example is a theoretical calculation in the change of the topology of graphene due to a circularly polarized electric field pulse [11] and another examined the transition metal dichalcogenides [17, 18]. But none of that work addressed the specific question of how long must a pulse be on before the system appears to be described by the Floquet limit. We do

so in chapter 3. Depending on the parameters, it turns out that the drive time need not be so long. Experimentally, this has been demonstrated with topological insulators [19].

In spite of the large interest in periodically driven many-body systems, rigorous statements about the properties of measurable and computable quantities in the Floquet regime are scarce. As a relevant example, we draw the reader's attention to the fact that the fermionic spectral density is nonnegative in equilibrium, allowing its interpretation as a probabilitistic density of states. But in Floquet systems, there is no *a priori* guarantee that a spectral density will be nonnegative. As a result, others have employed weighted sums over various elements of the response functions in the Floquet representation [13, 20–22], which have turned out to be nonnegative. But to our knowledge, no proof of nonnegativity has been offered. This is a nontrivial issue, as the standard approach to constructing spectral funtions, which involves using Wigner coordinates of average and relative time, and Fourier transforming the relative time to a frequency, produces spectral functions $\rho(\omega, t_{\text{ave}})$ that usually display negative values, as demonstrated in chapter 3. However, they become nonnegative after further averaging over t_{ave} [23, 24]. For noninteracting single-band models, analytical proofs do exist that show how averaging over one period T guarantees nonnegative spectral densities [25], which is also shown in chapter 3. Nevertheless, negative densities are sometimes seen for interacting systems [25], so far without explanation. This illustrates the need for tangible analytic results which hold also in presence of interactions.

We solve this problem in chapter 4 by deriving a spectral representation for retarded Green functions in the quasi-stationary Floquet regime. This spectral representation generalizes the well-established Lehmann representation of equilibrium quantum mechanics. Like the latter, our generalization allows one to derive rigorous general conclusions, e.g., on the nonnegativity of spectral functions and on their sum rules. For this reason, the derived results will guide many future studies in the field.

The remainder of the thesis is organized as follows: We start by introducing the basical properties of both Green functions and Floquet theory in chapter 2. In chapter 3 we focus on examining band electrons driven by an external electric field. The problem is solved exactly via the Peierls' substitution [26]. We focus on the limit of infinite dimensions, because it allows us to obtain a number of exact analytic relations. It also allows for this work to benchmark interacting calculations performed with nonequilibrium dynamical mean-field theory [27, 28] in the future. The model and the methodology used to solve for the retarded Green functions for different pulsed drives is introduced in section 3.1, before we present our numerical results for different pulsed drives in the rest of chapter 3. While chapter 3 focuses on noninteracting band electrons, we study more general, interacting systems in chapter 4. There, we generalize the proof of the nonnegativity of averaged spectral densities that we give in section 3.2 for interacting systems, which allows to study the properties of sum rules and of the self energy. For the latter, we compute the Dyson equation of periodically driven systems in section 4.2. Our conclusions are given in chapter 5, which also provides an outlook. An appendix about the formal properties of the convolution of two periodic functions and about the sum rules for higher moments of the spectral densities in the Hubbard model follows at the end.

2 Methods

Green functions are a crucial ingredient when studying systems in nonequilibrium, as they allow the calculation of spectral densities and contain information regarding the correlation of strongly correlated systems [29, 30]. Floquet theory follows the same concept as the more commonly known Bloch theory, but instead of making use of a potential that is periodic in space, it treats systems that are periodic in time. This means the Hamiltonian is time translational invariant in the Period T. Floquet theory is used to study strongly driven periodic quantum systems, and one of its advantages is that it respects this periodicity at all levels of the perturbation. Additionally no secular terms, meaning terms that are linear or not periodic in the time variable occur. [8]. Both methods will be employed throughout this thesis, therefore we will introduce them in this chapter. In order to simplify the equations, we will set the reduced Plank constant $\hbar$ to $\hbar = 1$ both in this chapter and when we are discussing interacting systems in chapter 4. We make an exception in chapter 3, where we will explicitly consider $\hbar$ in order to determine whether the magnitude of the parameters needed to reproduce the analytical results is realizable in an experiment.

2.1 Green functions

We consider a closed quantum mechanical system described by the time-dependent Hamiltonian $\mathcal{H}(t)$. Hence, any linear response function, e.g., a fermionic or bosonic progagator, depends on two times t_1 and t_2 in a non-trivial way. Kubo's formalism [31] tells us that a retarded response function is given by

$$G(t_1, t_2) := -i \left\langle \left[c(t_1), c^\dagger(t_2)\right]_\pm \right\rangle \Theta(t_1 - t_2), \tag{2.1}$$

where c can be any, possibly composite, fermionic or bosonic operator, e.g., a fermionic annihilation operator in position space or in momentum space or a Hubbard operator. If it is overall fermionic (that means odd in the number of fermionic creation or annihilation operators), the $+$ sign applies in the anticommutator $[\cdot]_+$; if it is overall bosonic, the $-$ sign applies in the commutator $[\cdot]_-$. In equilibrium, this retarded Green function is the only response function that needs to be considered, as all other Green functions can be constructed from the retarded one [32]. Never the less, it is useful to also consider the greater and the lesser Green function [33], given by

$$G^>(t_1, t_2) := -i \left\langle c(t_1) c^\dagger(t_2) \right\rangle \tag{2.2a}$$
$$G^<(t_1, t_2) := \pm i \left\langle c^\dagger(t_2) c(t_1) \right\rangle \tag{2.2b}$$

(the upper sign refers to fermions). We are interested in the retarded Green function [29], which can be derived from the greater and the lesser Green function by

$$G(t_1, t_2) = (G^{>}(t_1, t_2) - G^{<}(t_1, t_2))\Theta(t_1 - t_2)\,. \tag{2.3}$$

The density of states (DOS) is found from the temporal Fourier transform of the local retarded Green function. In equilibrium, where the Green function is only dependent on the relative time $t_1 - t_2$, it is unambiguous what is meant by the frequency-dependent response $G(\omega)$ which is obtained by computing the Fourier transform of $G^{\mathrm{R}}_{\mathrm{loc}}(t_1 - t_2)$. If, however, a driving that varies in time is applied to the system, the situation is different, as we have a two-time response $G^{\mathrm{R}}_{\mathrm{loc}}(t_1, t_2)$. In generic pump-probe experiments, frequency resolved quantities are measured as a function of the delay time.

Careful analysis of a given experiment will yield the proper way to integrate over time and construct the frequency-dependent response, as was done for photoemission in Ref. [34–36]. Nevertheless, when we examine Green functions, it is useful to represent them in terms of frequency irrespective of any particular measurement. This procedure is not unique, and we describe two particular ways to do it next.

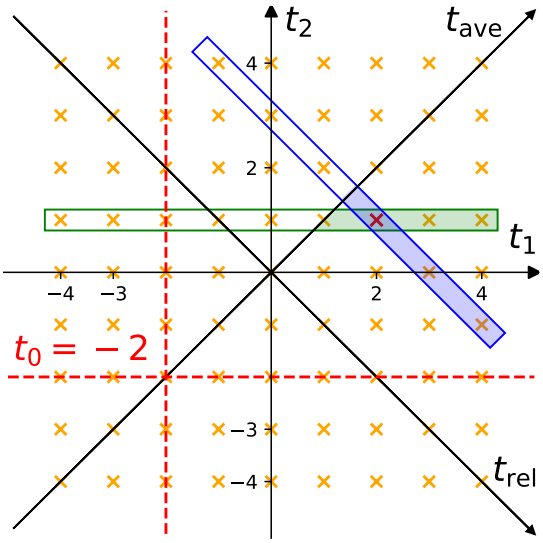

Figure 2.1: Schematic display of the two times for the Green function and the integration directions for the horizontal time and average time DOS. For retarded quantities, the Fourier transform runs only over the darker parts of the rectangles. Retarded quantities are nonzero only below and to the right of the diagonal labeled t_{ave}, defined by $t_{\mathrm{rel}} = 0$.

The first definition introduces the Wigner coordinates [37], where the Fourier transform is performed in the relative time $t_{\mathrm{rel}} = t_1 - t_2$ while the average time $t_{\mathrm{ave}} = (t_2 + t_1)/2$ is kept constant. The Green function is expressed as

$$G^{\mathrm{R}}_{\mathrm{loc}}(t_1, t_2) = G^{\mathrm{R}}_{\mathrm{loc}}\left(t_{\mathrm{ave}} + \frac{t_{\mathrm{rel}}}{2}, t_{\mathrm{ave}} - \frac{t_{\mathrm{rel}}}{2}\right)\,. \tag{2.4}$$

Figure 2.1 schematically displays the concept of these coordinates by introducing the diagonal axis for t_{ave} and t_{rel}. This means that all grid points on a line perpendicular to the diagonal axis for t_{ave} are associated with the same average time, just as all grid points perpendicular to the axis $t_{\text{rel}}/2$ have the same relative time. For example, the grid point $(t_1, t_2) = (2, 1)$, which is marked in red, has the average time $t_{\text{ave}} = 1.5$, and so do all the grid points in the blue rectangle. That is, it is exactly those times that the Fourier transformation is computed over when the average time is chosen to be $t_{\text{ave}} = 1.5$, which is why we will refer to this as the diagonal Fourier transform $\mathcal{F}_{\text{D}}$. It is employed to calculate the frequency dependent diagonal Green function via

$$G^{\text{R}}(\omega, t_{\text{ave}}) = \int_0^\infty e^{i\omega t_{\text{rel}}} G^{\text{R}}(t_{\text{ave}}, t_{\text{tel}})\, \mathrm{d}t_{\text{rel}}\,, \tag{2.5}$$

so the diagonal DOS yields

$$\rho_{\text{D}}(\omega, t_{\text{ave}}) = -\frac{1}{\pi}\text{Im}\left[G^{\text{R}}(\omega, t_{\text{ave}})\right]\,. \tag{2.6}$$

The above procedure is popular because t_{ave} can loosely be interpreted as the "time corresponding to the DOS" In this case it is reasonable to identify the time associated with the Fourier transform to be in the middle of the interval $[t_2, t_1]$.

There are potential problems with this choice. If the pulse starts at t_0, then for $t_{\text{ave}} < t_0$ there are traces of the effect of the pulse in the DOS even though t_{ave} is before the pulse was turned on. This is due to large enough positive t_{rel} contributions in the Green function given in Eq. (2.4) from times after the onset of the pulse ($t_1 > t_0$). The converse is also true. If $t_{\text{ave}} > t_0$, then for large enough t_{rel}, we have $t_2 < t_0$, so contributions to a field dressed DOS include terms before the field was turned on.

In Fig. 2.1, the dashed red line represents a pulse starting at $t_0 = -2$. Even if the average time is chosen to be $t_{\text{ave}} = 1.5$, the Fourier transformation with respect to $t_{\text{rel}} > 0$, displayed as the area shaded in blue, will eventually cross the dashed line and include values $t_2 < t_0$.

We can also define a horizontal Green function as

$$G^{\text{R}}_{\text{loc}}(t_1, t_2) = G^{\text{R}}_{\text{loc}}(t_{\text{rel}} + t_2, t_2)\,, \tag{2.7}$$

and again perform the Fourier transform in the relative time t_{rel}. In Figure 2.1, this is displayed as the green box, for all of the grid points in it satisfy $t_2 = 1$. This horizontal Fourier transform $\mathcal{F}_{\text{H}}$ yields the horizontal freuqency dependent Green function

$$G^{\text{R}}(\omega, t_2) = \int_0^\infty e^{i\omega t_{\text{rel}}} G^{\text{R}}_{\text{loc}}(t_{\text{rel}} + t_2, t_2)\, \mathrm{d}t_{\text{rel}} \tag{2.8}$$

and the horizontal density of states, given by

$$\rho_{\text{H}}(\omega, t_2) = -\frac{1}{\pi}\text{Im}\left[G^{\text{R}}(\omega, t_2)\right]\,. \tag{2.9}$$

The advantage of this definition is, that for $t_2 > t_0$, all times used for the Fourier transform occur after the onset of the pulse. That is, for $t_{\text{rel}} > 0$ the shaded green area in Fig. 2.1 will never cross the dashed red line. The disadvantage is that the average time is not fixed. Of course, in static equilibrium both response functions are equal and indistinguishable.

2.2 Floquet theory

Gaston Floquet was a French mathematician studying (amongst other things) the theory of differential equations. When quantum mechanics became popular in the first half of the 20^{th} century, Floquets results from *Sur les équations différentielles linéaires à coefficients périodiques* [6] in 1883 were applied to quantum mechanical systems with a periodic, time-dependent Hamiltonian

$$\mathcal{H}(t) = \mathcal{H}(t+T) \quad \forall\, t\,, \tag{2.10}$$

where T is the period in time, resulting in what today is known in physics as *Floquet theory*. The standard approach of this theory can be found in many textbooks and publications, such as Ref. [8] or Ref. [38]. It considers the Schrödinger equation for such periodic Hamiltonians

$$i\partial_t \left|\psi(t)\right\rangle = \mathcal{H}(t) \left|\psi(t)\right\rangle\,, \tag{2.11}$$

which is generally solved by the linear superposition of special solutions of the form [7, 8]

$$\left|\psi_m(t)\right\rangle = \exp(-i\epsilon_m t) \left|m,t\right\rangle \quad \forall\, m \in \mathbb{N}_0 \tag{2.12}$$

where the quasi-eigenstates $\left|m,t\right\rangle$ are periodic in time with period T:

$$\left|m,t+T\right\rangle = \left|m,t\right\rangle\,. \tag{2.13}$$

This ansatz strongly reminds of the Bloch theorem transferred to time. At any given instant t, the states $\left|m,t\right\rangle$ form a complete, orthonormal basis. They are the eigenstates of the modified Hamiltonian

$$\tilde{\mathcal{H}}\,(t) = \mathcal{H}\,(t) - i\partial_t\,, \tag{2.14}$$

and the quasi eqnergy ϵ_m is the corresponding Eigenvalue, satisfing

$$\tilde{\mathcal{H}} \left|m,t\right\rangle = \epsilon_m \left|m,t\right\rangle\,. \tag{2.15}$$

Therefore the modified quasi-eigenstates $\left|ml,t\right\rangle = \exp\left(i\frac{2\pi l}{T}t\right)\left|m,t\right\rangle$ obey

$$\tilde{\mathcal{H}} \left|ml,t\right\rangle = \exp\left[i\frac{2\pi}{T}l\right] \mathcal{H}\,(t) \left|m,t\right\rangle - i\exp\left[i\frac{2\pi l}{T}t\right] \partial_t \left|m,t\right\rangle - i\left(\partial_t \exp\left[i\frac{2\pi l}{T}t\right]\right)\left|m,t\right\rangle \tag{2.16a}$$

$$= \exp\left[i\frac{2\pi l}{T}t\right] \left(\mathcal{H}\,(t) - i\partial_t\right)\left|m,t\right\rangle - i\left(i\frac{2\pi l}{T}\exp\left[i\frac{2\pi l}{T}t\right]\right)\left|m,t\right\rangle \tag{2.16b}$$

$$= \left(\tilde{\mathcal{H}}\,(t) + \frac{2\pi l}{T}\right)\exp\left[i\frac{2\pi l}{T}t\right]\left|m,t\right\rangle \tag{2.16c}$$

$$= \left(\epsilon_m + \frac{2\pi l}{T}\right)\left|ml,t\right\rangle\,, \tag{2.16d}$$

meaning the modified quasi-eigenstates yield the same solution with a shifted quasi-energy. The quasi-energy ϵ_m is uniquely defined only if it is restricted to the interval $\epsilon_m \in (-\pi/T, \pi/T]$. This is the temporal equivalent of a Brillouin zone.

Even though the approach presented above is commonly used in quantum mechanics, we find it more insightful to derive the above results differently, starting by considering the

unitary time evolution operator $U(t_1, t_2)$ and in particular $U(T, 0)$. Any unitary operator such as $U(T, 0)$ has an orthonormal eigen basis $\{|\psi_m\rangle\}$, which we do not yet identify with the Floquet state solutions in (2.12), fulfilling

$$U(T,0)\,|\psi_m\rangle = \lambda_m\,|\psi_m\rangle\ . \tag{2.17}$$

Since $U(T, 0)$ is unitary the absolute value of λ_m is unity so that it can be written as

$$\lambda_m = \exp(-i\epsilon_m T) \tag{2.18}$$

where again the quasi-energy ϵ_m has to be restricted to the interval $\epsilon_m \in (-\pi/T, \pi/T]$ in order to be uniquely defined. Next, we take the states $|\psi_m\rangle$ as initial states, i.e., $|\psi_m(t=0)\rangle = |\psi_m\rangle$ for a time-evolution according to the Schrödinger equation (2.11). We emphasize that the orthonormality and the completeness persist in the course of the time evolution because it is unitary

$$\langle\psi_m(t)|\ \psi_n(t)\rangle = \delta_{mn} \tag{2.19a}$$

$$\sum_m |\psi_m(t)\rangle\,\langle\psi_m(t)\rangle = \mathbb{1}. \tag{2.19b}$$

But these relations only hold if the time arguments in bra and ket are the same. Since the states $|\psi_m(t)\rangle$ are solutions of the Schrödinger equation

$$U(t_1,t_2)\,|\psi_m(t_2)\rangle = |\psi_m(t_1)\rangle \tag{2.20}$$

holds by definition for all times t_1 and t_2. Thus, the unitary time evolution is given by as

$$U(t_1,t_2) = \sum_m |\psi_m(t_1)\rangle\,\langle\psi_m(t_2)|\,. \tag{2.21}$$

One can verify that this solves the Schrödinger equation

$$i\partial_{t_1}U(t_1,t_2) = i\partial_{t_1}U(t_1,t_2)\sum_m |\psi_m(t_2)\rangle\,\langle\psi_m(t_2)| \tag{2.22a}$$

$$= \sum_m i\partial_{t_1}\,|\psi_m(t_1)\rangle\,\langle\psi_m(t_2)| \tag{2.22b}$$

$$= \sum_m \mathcal{H}(t_1)\,|\psi_m(t_1)\rangle\,\langle\psi_m(t_2)| \tag{2.22c}$$

$$= \mathcal{H}(t_1)U(t_1,t_2)\,. \tag{2.22d}$$

where we used that the states $\langle\psi_m(t_1)|$ fulfill the Schrödinger equation (2.11). The initial condition

$$U(t_2,t_2) = \mathbb{1} \tag{2.23}$$

is fulfilled due to the completeness (2.19b) of the states $\{|\psi_m(t)\rangle\}$. From Eq. (2.21) it is easy to derive that the product of two time evolution operators is given by

$$U(t_1,t_2)U(t_2,t_3) = \sum_{m,n} |\psi_m(t_1)\rangle\,\langle\psi_m(t_2)|\ \psi_n(t_2)\rangle\,\langle\psi_n(t_3)\rangle \tag{2.24a}$$

$$= \sum_m |\psi_m(t_1)\rangle\,\langle\psi_m(t_3)| \tag{2.24b}$$

$$= U(t_1,t_3)\,, \tag{2.24c}$$

and that the conjugate transpose is given by

$$U^\dagger(t_1, t_2) = U(t_2, t_1)\,. \tag{2.25}$$

By construction (2.17), the property

$$|\psi_m(T)\rangle = U(T, 0)\,|\psi_m\rangle = \exp(-i\epsilon_m T)\,|\psi_m\rangle \tag{2.26}$$

holds. More generally, quasi-periodicity holds

$$\begin{aligned} |\psi_m(t+T)\rangle &= U(t+T, 0)\,|\psi_m\rangle && \text{(2.27a)}\\ &= U(t+T, T)U(T, 0)\,|\psi_m\rangle && \text{(2.27b)}\\ &= U(t+T, T)\,|\psi_m\,(T)\rangle && \text{(2.27c)}\\ &= U(t, 0)\exp(-i\epsilon_m T)\,|\psi_m\rangle && \text{(2.27d)} \end{aligned}$$

resulting from the periodicity of the unitary time evolution which in turn is implied by the periodicity of the Hamiltonian and of (2.17). Combining the unitary operator and the ket in (2.27d) yields

$$|\psi_m(t+T)\rangle = \exp(-i\epsilon_m T)\,|\psi_m(t)\rangle \tag{2.28}$$

which confirms that $|\psi_m(t)\rangle$ is periodic *up to the factor* $\exp(-i\epsilon_m T)$. This is what is conventionally regarded as the Floquet theorem.

Finally, we define the states used in (2.12)

$$|m, t\rangle \coloneqq \exp(i\epsilon_m t)\,|\psi_m(t)\rangle\,. \tag{2.29}$$

Clearly, these states are periodic inheriting this property from the quasi-periodicity (2.28) of $|\psi_m(t)\rangle$. Equally, they form an orthonormal basis

$$\begin{aligned} \langle m, t|\, n, t\rangle &= \delta_{mn} && \text{(2.30a)}\\ \sum_m |m, t\rangle\,\langle m, t| &= \mathbb{1}. && \text{(2.30b)} \end{aligned}$$

which results again from the orthonormality (2.19) of the states $|\psi_m(t)\rangle$.

The representation of the time evolution operator (2.21) can be expressed in terms of the states $|m, t\rangle$ as well

$$U(t_1, t_2) = \sum_m \exp(-i\epsilon_m(t_1 - t_2))\;|m, t_1\rangle\,\langle m, t_2|\;. \tag{2.31}$$

3 Noninteracting lattice fermions driven by light pulses

As desribed in section 2.2, Floquet theory is applicable for quantum systems with a Hamiltonian that is invariant under time translations $t \to t + t_{\text{period}}$, i.e. a Hamiltonian being a periodic function in time with the period t_{period} [7]. This only holds for systems that are exposed to a driving field that is strictly periodic in time, meaning it is turned on at $t = -\infty$ and stays on. It is obvious that such a driving can never be realized in an experiment. Therefore in this chapter we will be comparing the properties of the DOS of lattice fermions coupled to an infinite sinusoidal driving to the DOS of three field pumps that are not strictly periodic, but are experimentally feasible. The field pumps we will be considering, namely a semi-infinite driving starting ar $t_0 = 0$, a sinusoidal steplike pulse and a sinusoidal drive with a Gaussian envelope, are displayed in Fig. 3.1.

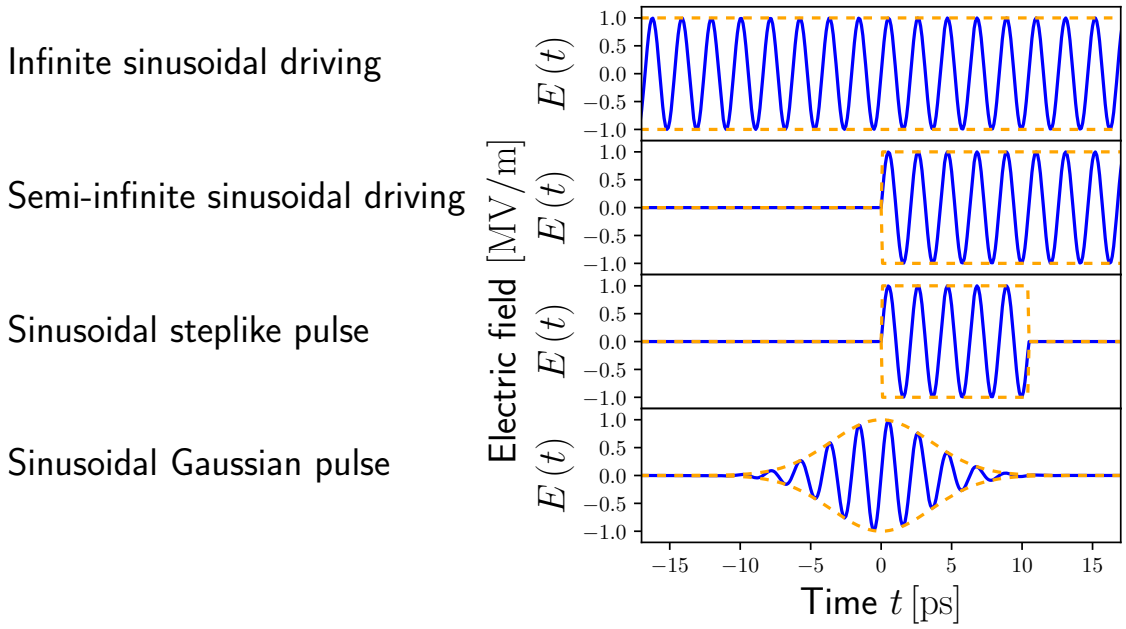

Figure 3.1: Schematic display of the driving fields (blue) that are discussed in this chapter and the envelope functions (orange) that are used to model the sinusoidal drive. The amplitude E is given as a function of the time t, which is displayed in units of picoseconds, since pump-probe experiments usually apply driving frequencies in the order of terahertz. In this figure the driving frequency it is arbitrarily set to $\Omega = 3\text{THz}$, and we chose the lattice spacing to be $a = 100\text{pm}$. The maximal amplitude is set to $E^{\max} = 1\text{MV/m}$, which can be realized in pump-probe experiments (for details, see section 3.2 and Refs. [39, 40]). Those parameters as well as the width of the steplike pulse and the Gaussian envelope will be varied throughout this thesis.

3.1 Model

We illustrate next how to describe lattice fermions under the influence of an external field. We start with the tight-binding Hamiltonian [41] in the absence of a field given by

$$\mathcal{H}_0 = -\sum_{ij=1}^{N} t_{ij} c_i^\dagger c_j - \mu \sum_{i=1}^{N} c_i^\dagger c_i \,, \tag{3.1}$$

where t_{ij} is the hermitian hopping matrix, μ is the chemical potential, and N is the number of lattice sites. The fermionic annihilation operator c_j destroys an electron at lattice site j while the fermionic creation operator $c_i^\dagger$ creates an electron at lattice site i. In this paper, we assume spinless electrons, and nearest-neighbor hopping on a hypercubic lattice in $d \to \infty$ dimensions. The nonzero elements t_{ij} of the hopping matrix are given by

$$t_{ij} = \frac{t^*}{2\sqrt{d}} \tag{3.2}$$

[42], and depend on the rescaled hopping constant t^*. We couple this system to an external electromagnetic field described by

$$\boldsymbol{E}(\boldsymbol{r},t) = -\boldsymbol{\nabla}\Phi(\boldsymbol{r},t) - \frac{1}{c}\frac{\partial \boldsymbol{A}(\boldsymbol{r},t)}{\partial t} \,, \tag{3.3}$$

where $\Phi(\boldsymbol{r},t)$ is a scalar potential and $\boldsymbol{A}(\boldsymbol{r},t)$ is a vector potential. The speed of light is c, and we use the Hamiltonian gauge [43] to set the scalar potential $\Phi(\boldsymbol{r},t) = 0$. The electric field effect on the hopping matrix is taken into account by performing the Peierls' substitution [44]. The original matrix element is multiplied by the exponential of the integral over the vector potential from the lattice vector $\boldsymbol{R}_i$ to the lattice vector $\boldsymbol{R}_j$ as follows:

$$t_{ij} \to t_{ij} \exp\left(-\frac{ie}{\hbar c}\int_{\boldsymbol{R}_i}^{\boldsymbol{R}_j} \boldsymbol{A}(\boldsymbol{r},t)\ \mathrm{d}\boldsymbol{r}\right) . \tag{3.4}$$

Here, the absolute value of the electron charge is given by e. This Peierls' substitution is for a single band model, which means there are no dipole transitions between bands [33]. While the electric fields we are considering vary in time, we assume they are spatially uniform, so the magnetic field associated with them is negligible and $\boldsymbol{A}(\boldsymbol{r},t) \to \boldsymbol{A}(t)$. This assumption can be made because the wavelength of the driving field is much larger then the atomic scales. In this case, the momentum-space representation for the Hamiltonian of noninteracting electrons coupled to a spatially uniform electric field can be written as a function of the band structure

$$\varepsilon(\boldsymbol{k}) = -\frac{t^*}{\sqrt{d}}\sum_{\alpha=1}^{d}\cos(k_\alpha a) \,, \tag{3.5}$$

where a is the lattice constant. The momentum-space Hamiltonian becomes

$$\mathcal{H}(t) = \sum_{\boldsymbol{k}}\left[\varepsilon\left(\boldsymbol{k} - \frac{e\boldsymbol{A}(t)}{\hbar c}\right) - \mu\right] c_{\boldsymbol{k}}^\dagger c_{\boldsymbol{k}} \,, \tag{3.6}$$

with

$$c_{\boldsymbol{k}}^{\dagger} = \frac{1}{\sqrt{N}} \sum_{n=1}^{N} \exp\left[-i\boldsymbol{R}_n \boldsymbol{k}\right] c_n^{\dagger} \tag{3.7}$$

and the hermitian conjugate equation for c_k. For many driving fields, such as an electric field that is periodic in time, the Hamiltonian in Eq. (3.6) is a Floquet Hamiltonian. It has periodic time dependence due to the time dependence it inherits from the electric field. However, because the Hamiltonian with the Peierls' substitution is diagonal in momentum space, it commutes with itself for all times $[\mathcal{H}(t), \mathcal{H}(t')] = 0$. This greatly simplifies the problem. We consider the momentum-space representation of the creation and the annihilation operator in the Heisenberg picture, where $c_{\boldsymbol{k}}(t) = \exp\left[it\mathcal{H}(t)\right] c_{\boldsymbol{k}} \exp\left[-it\mathcal{H}(t)\right]$, and use the Hamiltonian in Eq. (3.6) to derive their time evolution, yielding

$$c_{\boldsymbol{k}}(t) = \exp\left[-\frac{i}{\hbar}\int_{-\infty}^{t}\left[\varepsilon\left(\boldsymbol{k} - \frac{e\boldsymbol{A}(t)}{\hbar c}\right) - \mu\right] \mathrm{d}t\right] c_{\boldsymbol{k}} \,. \tag{3.8}$$

This result allows us to analytically calculate the retarded momentum-dependent Green function, which is defined by

$$G^{\mathrm{R}}(\boldsymbol{k}, t_1, t_2) = -\frac{i}{\hbar}\Theta(t_1 - t_2)\left\langle\left\{c_{\boldsymbol{k}}(t_1), c_{\boldsymbol{k}}^{\dagger}(t_2)\right\}_{+}\right\rangle \,. \tag{3.9}$$

The angular brackets denote thermal averaging $\langle O\rangle = \mathrm{Tr}\left[\exp\left(-\beta\mathcal{H}_0\right) O\right] / \mathrm{Tr}\left[\exp\left(-\beta\mathcal{H}_0\right)\right]$, where the inverse temperature is given by $\beta = 1/T$ and $\mathcal{H}_0$ is the field-free Hamiltonian in Eq. (3.1). Using the time evolution of of the creation and the annihilation operator given in Eq. (3.8), this yields

$$G^{\mathrm{R}}(\boldsymbol{k}, t_1, t_2) = -\frac{i}{\hbar}\Theta(t_1 - t_2)\, e^{\frac{i\mu}{\hbar}(t_1 - t_2)} \exp\left[-\frac{i}{\hbar}\int_{t_2}^{t_1} \varepsilon\left(\boldsymbol{k} - \frac{eaA(t)}{\hbar c}\right) \mathrm{d}t\right] \left\langle c_{\boldsymbol{k}} c_{\boldsymbol{k}}^{\dagger} + c_{\boldsymbol{k}}^{\dagger} c_{\boldsymbol{k}}\right\rangle \,. \tag{3.10}$$

With the Fermi-Dirac distribution being $f(x) = 1/\left[1 + \exp(\beta x)\right]$, the creation and the annihilation operator satisfy $\left\langle c_{\boldsymbol{k}}^{\dagger} c_{\boldsymbol{k}}\right\rangle = f\left(\varepsilon(\boldsymbol{k}) - \mu\right)$ and $\left\langle c_{\boldsymbol{k}} c_{\boldsymbol{k}}^{\dagger}\right\rangle = 1 - f\left(\varepsilon(\boldsymbol{k}) - \mu\right)$, so it is obvious that $\left\langle c_{\boldsymbol{k}} c_{\boldsymbol{k}}^{\dagger} + c_{\boldsymbol{k}}^{\dagger} c_{\boldsymbol{k}}\right\rangle = 1$ [33]. To calculate the momentum-dependent Green function in Eq. (3.9), we specialize to a vector potential that lies along the diagonal, introducing a scalar function $A(t)$ that is associated with the vector potential via $\boldsymbol{A}(t) = A(t)(1, 1, 1, \ldots)$. In this case, the altered band structure is given by

$$\varepsilon\left(\boldsymbol{k} - \frac{eaA(t)}{\hbar c}\right) = \varepsilon(\boldsymbol{k}) \cos\left(\frac{eaA(t)}{\hbar c}\right) + \tilde{\varepsilon}(\boldsymbol{k}) \sin\left(\frac{eaA(t)}{\hbar c}\right) \,, \tag{3.11}$$

using the complementary energy function

$$\tilde{\varepsilon}(\boldsymbol{k}) = -\frac{t^*}{\sqrt{d}} \sum_{\alpha=1}^{d} \sin\left(k_\alpha a\right) \,, \tag{3.12}$$

which is the projection of the band velocity along the field direction. The retarded momentum-dependent Green function is then given by

$$\begin{aligned} G^{\mathrm{R}}\left(\boldsymbol{k}, t_1, t_2\right) &= -\frac{i}{\hbar}\Theta\left(t_1 - t_2\right) e^{\frac{i\mu}{\hbar}\left(t_1 - t_2\right)} \\ &\quad \times \exp\left[-i\frac{\varepsilon\left(\boldsymbol{k}\right)}{\hbar}\int_{t_2}^{t_1} \cos\left(\frac{eaA\left(t\right)}{\hbar c}\right) \mathrm{d}t\right] \\ &\quad \times \exp\left[-i\frac{\tilde{\varepsilon}\left(\boldsymbol{k}\right)}{\hbar}\int_{t_2}^{t_1} \sin\left(\frac{eaA\left(t\right)}{\hbar c}\right) \mathrm{d}t\right]. \end{aligned} \tag{3.13}$$

Of course this retarded Green function is independent of temperature as expected for Green functions of noninteracting systems. Note that in equilibrium the Hamiltonian is constant in time and hence the whole problem is time-translation invariant. Thus, only time differences matter and the Green function depends solely on the relative time $t_{\mathrm{rel}} = t_1 - t_2$. However, due to the coupling of the lattice fermions to a time-dependent electric field, the Green function in Eq. (3.13) depends separately on the time t_2 of the creation operator and the time t_1 of the annihilation operator. The local Green function can be computed by summing over all momentum vectors $\boldsymbol{k}$, which corresponds to the integration over ε and $\tilde{\varepsilon}$ respectively, by using the joint density of states for tight binding electrons on a hypercubic lattice

$$\rho_0\left(\varepsilon, \tilde{\varepsilon}\right) = \left(\frac{1}{\sqrt{\pi} t^* a^d}\right)^2 \exp\left[-\left(\frac{\varepsilon}{t^*}\right)^2 - \left(\frac{\tilde{\varepsilon}}{t^*}\right)^2\right]. \tag{3.14}$$

For an arbitrary function $\tilde{I}\left(t_1, t_2\right) \in \mathbb{R}$, the integral over ε can be calculated by completing the square, which leads to

$$\frac{1}{\sqrt{\pi} t^*}\int \mathrm{d}\varepsilon \exp\left[-\left(\frac{\varepsilon}{t^*}\right)^2 - \frac{i\varepsilon\tilde{I}\left(t_1, t_2\right)}{\hbar}\right] = \exp\left[-\left(\frac{t^*\tilde{I}\left(t_1, t_2\right)}{2\hbar}\right)^2\right]. \tag{3.15}$$

Additionally the identity

$$\left|\int_{t_2}^{t_1} \cos\left(\frac{eaA\left(t\right)}{\hbar c}\right) \mathrm{d}t\right|^2 + \left|\int_{t_2}^{t_1} \sin\left(\frac{eaA\left(t\right)}{\hbar c}\right) \mathrm{d}t\right|^2 = \left|\int_{t_2}^{t_1} \exp\left[\frac{ieaA\left(t\right)}{\hbar c}\right] \mathrm{d}t\right|^2 \tag{3.16}$$

is used to compute the local Green function, yielding

$$g^{\mathrm{R}}_{\mathrm{loc}}\left(t_1, t_2\right) = -\frac{i}{\hbar}\Theta\left(t_1 - t_2\right) e^{\frac{i\mu}{\hbar}\left(t_1 - t_2\right)} e^{-\left(\frac{t^*}{2\hbar}\right)^2 \left|I\left(t_1, t_2\right)\right|^2}, \tag{3.17}$$

where $I\left(t_1, t_2\right)$ is given by

$$I\left(t_1, t_2\right) = \int_{t_2}^{t_1} \exp\left[\frac{ieaA\left(t\right)}{\hbar c}\right] \mathrm{d}t\,. \tag{3.18}$$

In this paper, we will assume half filling ($\mu = 0$), so the time-dependent local Green function in Eq. (3.17) is purely imaginary.

3.2 Infinite sinusoidal driving

For the infinite sinusoidal driving with the frequency Ω and the amplitude E, the vector potential is given by

$$A_\infty(t) = \frac{cE}{\Omega}\cos(\Omega t)\ , \tag{3.19}$$

whose simple form enables the analytic determination of the local Green function. If we define the modified amplitude $E_0 = eaE/\hbar$, the squared absolute value of $I(t_1, t_2)$ in Eq. (3.18) yields

$$\left|I_\infty(t_1,t_2)\right|^2 = \frac{1}{\Omega^2}\left|\int_{t_2\Omega}^{t_1\Omega} f_c(t)\ \mathrm{d}t\right|^2 + \frac{1}{\Omega^2}\left|\int_{t_2\Omega}^{t_1\Omega} f_s(t)\ \mathrm{d}t\right|^2 \tag{3.20}$$

with the integrands

$$f_c(t) = \cos\left(\frac{E_0}{\Omega}\cos(t)\right) \tag{3.21a}$$

$$f_s(t) = \sin\left(\frac{E_0}{\Omega}\cos(t)\right)\ . \tag{3.21b}$$

Both $f_c(t)$ and $f_s(t)$ are even functions that are 2π-periodic, therefore they can be expressed as Fourier series with the Fourier coefficients c_m and s_m according to

$$f_c(t) = \frac{c_0}{2} + \sum_{m=1}^{\infty} c_m \cos(mt) \tag{3.22a}$$

$$f_s(t) = \sum_{m=1}^{\infty} s_m \cos(mt)\ . \tag{3.22b}$$

Note that due to the fact that $f_s(t)$ is not only 2π-periodic, but also π-anti-periodic, the coefficient s_0 vanishes, while the π-periodic function $f_c(t)$ has the coefficient $c_0 = 2J_0(E_0/\Omega)$, where J_α is the Bessel function of the first kind. Using the two $2\pi/\Omega$-periodic functions derived from integrating the Fourier coefficients of f_c and f_s,

$$\phi_c(t) = \frac{1}{\Omega}\sum_{m=1}^{\infty}\frac{c_m}{m}\sin(m\Omega t) \tag{3.23a}$$

$$\phi_s(t) = \frac{1}{\Omega}\sum_{m=1}^{\infty}\frac{s_m}{m}\sin(m\Omega t)\ , \tag{3.23b}$$

the integration in Eq. (3.20) can now easily be computed, yielding

$$\left|I_\infty(t_1,t_2)\right|^2 = \left|\phi_s(t_1) - \phi_s(t_2)\right|^2 + \left|J_0\left(\frac{E_0}{\Omega}\right)t_{\mathrm{rel}} + \phi_c(t_1) - \phi_c(t_2)\right|^2 . \tag{3.24}$$

In this form, it is obvious that the increase in $\left|I_\infty(t_1,t_2)\right|^2$ for large relative times is solely caused by the term dependent on the Bessel function and proportional to t_{rel}^2; a large $\left|I_\infty(t_1,t_2)\right|^2$ corresponds to a small Green function as seen in Eq. (3.17). This is because the periodic functions ϕ merely oscillate in time. Hence, if the amplitude and the frequency

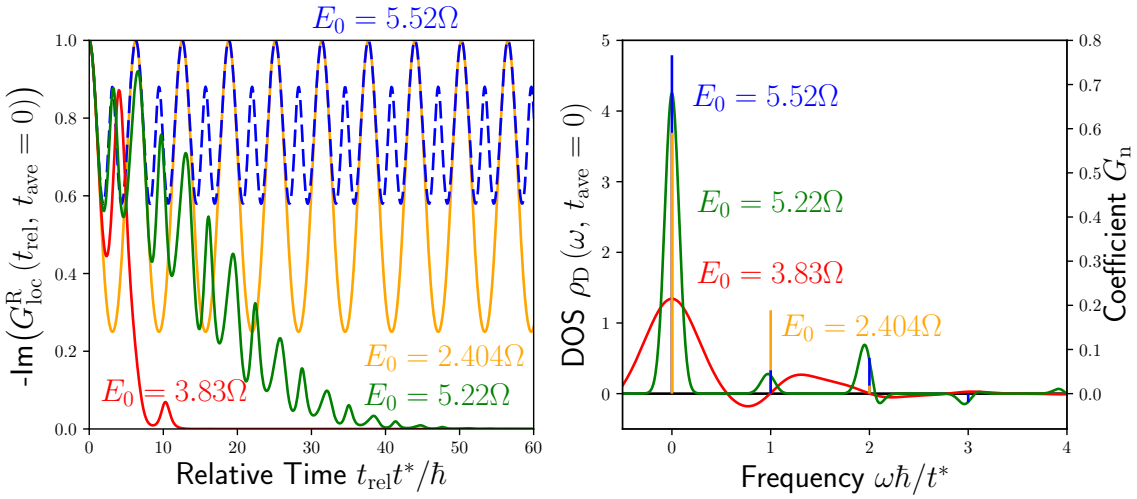

Figure 3.2: Left panel: Negative imaginary part of the local retarded Green function as a function of the relative time t_{rel} in units of the inverse rescaled hopping $\hbar/t^*$. Note that the real part vanishes because $\mu = 0$. Right panel: Diagonal DOS as a function of the frequency ω in units of the rescaled hopping. Because the DOS is a set of delta functions at $J_0\left(E_0/\Omega\right) = 0$ the coefficients $g_{\mathrm{n}} = -1/\left(2\pi\right)\int_0^{2\pi} \mathrm{d}t_{\mathrm{rel}}\mathrm{Im}\left[G^{\mathrm{R}}_{\mathrm{loc}}\left(t_{\mathrm{rel}}, 0\right)\right]\cos\left(nt_{\mathrm{rel}}\right)$ of the Fourier series are displayed for $E_0 = 2.404\Omega$ and $E_0 = 5.52\Omega$. Other parameters: average time $t_{\mathrm{ave}} = 0$, driving frequency $\Omega = t^*/\hbar$.

of the driving field are chosen in such a way that the Bessel function $J_0\left(E_0/\Omega\right)$ is zero, then the dephasing of the Green function, corresponding to the decay of $G^{\mathrm{R}}_{\mathrm{loc}}\left(t_1, t_2\right)$ for large t_{rel}, no longer occurs.

Figure 3.2 shows the imaginary part of the time-dependent local Green function at $t_{\mathrm{ave}} = 0$, as defined in Eq. (2.4) for different amplitudes of the electric field, while the frequency is kept constant at $\Omega = t^*/\hbar$. Note that the Green function at half filling is purely imaginary [see Eq. (3.17)]. In this case, the absolute value of Bessel function is purely dependent on the amplitude of the driving. If the amplitude is chosen to be $E_0 = 2.404\Omega$, which corresponds to the first zero of the Bessel function (displayed in orange), it is clear that there is no dephasing in t_{rel} and the local Green function oscillates with a period of $2\pi/\Omega$ between one and a constant value less than one. Note that if the Bessel function is zero, the squared absolute value of $I_\infty\left(t_1, t_2\right)$ in Eq. (3.24) is merely a superposition of sinusoidal functions that are periodic in $2\pi/\Omega$. This means the DOS is a set of delta functions and the dominant frequencies are $\omega = 0$ and $\omega = \pm\Omega$. The next zero of the Bessel function occurs at $E_0 = 5.52\Omega$, and again the imaginary part oscillates with a period of $2\pi/\Omega$ around a constant value. However, the amplitude changes and additional peaks appear. Therefore the DOS is again a set of delta functions, but it consists of more delta peaks than at the first zero. This behavior continues, as the amplitude takes values of higher zeros of the Bessel function.

The imaginary part of the Green function at a constant $t_2 = 0$ [as defined in Eq. (2.7)] shows the same overall properties when displayed as a function of t_{rel}, differences being that the lower extreme value shifts and the oscillations have double the frequency. This

behavior can easily be understood, because in Eq. (3.24) t_1 and t_2 are the arguments of the function ϕ, where they solely appear in the argument of the sine function. But in the average time Green function (2.4), both t_1 and t_2 are dependent on $t_{\mathrm{rel}}/2$, while they are dependent on t_{rel} without an additional factor in the Green function for the horizontal case (2.7). Therefore the period of the oscillations in t_{rel} for a constant t_{ave} is twice as large for a constant t_2.

Contrary to the behavior at the zeros of the Bessel function, the dephasing in t_{rel} is fast at extreme values of the Bessel function like its first minimum at $E_0 = 3.83\Omega$, which is displayed in red, because the squared absolute value of $|I_\infty(t_1, t_2)|^2$ is large, even if t_{rel} is still comparatively small. As the argument of the Bessel function becomes smaller, the dephasing takes longer.

But is it even possible in a pump-probe experiment to measure at frequencies and amplitudes that allow to reach the first zero of the Bessel function? If we assume the driving frequency to be in the order of terahertz, which is common for pump-probe experiments ($\Omega \propto 10^{12}\mathrm{s}^{-1}$), the amplitude of the electric field would need to be $E = 2.404\,\Omega\hbar/(ea) \approx 15 \times 10^6 \mathrm{V/m}$ as the first zero of the Bessel function is at $J_0(2.404) = 0$. Amplitudes of that magnitude can indeed be realized in pump-probe experiments, one example can be found in Refs. [39, 40]

For a time-independent Hamiltonian it is easy to prove that the DOS is positive semidefinite, via the Lehmann representation. However, this is not necessarily the case for the DOS of a driven system where the DOS takes negative values if it is computed at a constant t_{ave} or t_2. One can even argue if it is correct to call a spectral function that takes negative values DOS, because it cannot be interpreted physically as such. We will make a more specific distinction in chapter 4, but for now continue to call the spectral function defined by $\rho(\omega, t_{\mathrm{ave}}) := -\pi^{-1}\mathrm{Im}G(\omega, t_{\mathrm{ave}})$ DOS, in order to keep the notation, especially in the figures, simple.

For a pure Floquet Hamiltonian the DOS has to be periodic in the Floquet period, which is the period of the driving, and averaging over this Floquet period in t_{ave} or t_2, respectively, does lead to a semidefinite DOS. To show this analytically, we consider the retarded Green function at half filling, introduced in Eq. (3.13) and write it in terms of the functions ϕ introduced in Eq. (3.23), yielding

$$\begin{aligned} G^{\mathrm{R}}(\boldsymbol{k}, t_1, t_2) &= -\frac{i}{\hbar}\Theta(t_1 - t_2)\exp\left[-\frac{i}{\hbar}\varepsilon(\boldsymbol{k})\, J_0\left(\frac{E_0}{\hbar}\right)(t_1 - t_2)\right] && (3.25)\\ &\quad \times\exp\left[-\frac{i}{\hbar}\left(\varepsilon(\boldsymbol{k})\,\phi_c(t_1) - \varepsilon(\boldsymbol{k})\,\phi_c(t_2)\right)\right] \\ &\quad \times\exp\left[-\frac{i}{\hbar}\left(\tilde{\varepsilon}(\boldsymbol{k})\,\phi_s(t_1) - \tilde{\varepsilon}(\boldsymbol{k})\,\phi_s(t_2)\right)\right]. && (3.26) \end{aligned}$$

Defining the $2\pi/\Omega$ periodic function $\Phi(t, \boldsymbol{k})$

$$\begin{aligned} \Phi(t, \boldsymbol{k}) &= \exp\left[-\frac{i\varepsilon(\boldsymbol{k})}{\hbar}\phi_c(t) - \frac{i\tilde{\varepsilon}(\boldsymbol{k})}{\hbar}\phi_s(t)\right] && (3.27a)\\ &= \sum_m e^{im\Omega t} f_m(\boldsymbol{k}) && (3.27b) \end{aligned}$$

allows us to write this Green function as

$$\begin{aligned} G^{\mathrm{R}}\left(\boldsymbol{k}, t_{\mathrm{ave}}, t_{\mathrm{rel}}\right) &= -\frac{i}{\hbar}\exp\left[-\frac{i\varepsilon\left(\boldsymbol{k}\right)}{\hbar}J_0\left(\frac{E_0}{\hbar}\right)t_{\mathrm{rel}}\right]\Theta\left(t_{\mathrm{rel}}\right) \\ &\quad\times\Phi^*\left(t_{\mathrm{ave}}-\frac{t_{\mathrm{rel}}}{2},\boldsymbol{k}\right)\Phi\left(t_{\mathrm{ave}}+\frac{t_{\mathrm{rel}}}{2},\boldsymbol{k}\right). \end{aligned} \tag{3.28}$$

As shown in Appendix A, using the convolution of two $2\pi/\Omega$ periodic functions and the fact that Φ can be written as a Fourier series with the coefficients f_m, the integral over one period is given by

$$\frac{\Omega}{2\pi}\int_x^{x+\frac{2\pi}{\Omega}}\Phi^*\left(\tilde{t}-\frac{t}{2}\right)\Phi\left(\tilde{t}+\frac{t}{2}\right)\mathrm{d}\tilde{t}=\sum_m |f_m|^2 e^{imt\Omega}. \tag{3.29}$$

Note that we are suppressing the $\boldsymbol{k}$ dependence of both Φ and f_m in order to simplify the notation.

This allows us to compute the averaged Green function

$$\bar{G}^R\left(\boldsymbol{k}, t_{\mathrm{rel}}\right)=\frac{\Omega}{2\pi}\int_x^{x+\frac{2\pi}{\Omega}} G^R\left(\boldsymbol{k},\tau,t_{\mathrm{rel}}\right)\mathrm{d}\tau \tag{3.30}$$

and the averaged spectral function $\bar{\rho}\left(\omega,\boldsymbol{k}\right)$, yielding

$$\bar{\rho}\left(\omega,\boldsymbol{k}\right) = -\frac{1}{\pi}\mathrm{Im}\left(\int_0^\infty e^{i\omega t_{\mathrm{rel}}}\bar{g}^R\left(\boldsymbol{k},t_{\mathrm{rel}}\right)\mathrm{d}t_{\mathrm{rel}}\right) \tag{3.31a}$$

$$= \frac{1}{\hbar}\sum_m |f_m|^2\delta\left(\omega+m\Omega-\frac{\varepsilon\left(\boldsymbol{k}\right)}{\hbar}J_0\left(\frac{E_0}{\hbar}\right)\right) \tag{3.31b}$$

which is indeed nonnegative for all ω. While the diagonal and the horizontal DOS corresponding to the infinite sinusoidal driving are different at a given time t_2 for the horizontal DOS and t_{ave} for the diagonal DOS (even if $t_2 = t_{\mathrm{ave}}$), the time-averaged spectral function $\bar{A}\left(\omega,\boldsymbol{k}\right)$ (and therefore the DOS averaged over the Floquet period) are always the same. Details can be found in Appendix A.

3.3 Semi-infinite sinusoidal driving starting at $t_0 = 0$

While a driving field that is switched on at a given time $t_0 = 0$ but stays on is also not experimentally implementable, it is useful to study the properties of its DOS because there are many similarities to the behavior of the DOS of driving pulses that can be experimentally implemented (see below). The vector potential of this semi-infinite sinusoidal driving is given by $A = (cE/\Omega)\cos\left(\Omega t\right)\Theta\left(t\right) - (cE/\Omega)\,\Theta\left(t\right)$. Again, the simple form of this expression allows us to analytically calculate the local retarded Green function in Eq. (3.17). For this driving, one has to distinguish between three time intervals when calculating the absolute value squared of $I\left(t_1,t_2\right)$. If both the annihilation operator at t_1 and the creation operator at t_2 are applied before the field is switched on, i.e. $t_2 < t_1 < 0$, the Hamiltonian equals a tight-binding Hamiltonian without an electric field as given in Eq. (3.1). In this case,

$I(t_1, t_2) = t_{\text{rel}}$ and the local Green function in Eq. (3.17) is a Gaussian in t_{rel} multiplied by a step function, which becomes the Gaussian DOS after Fourier transformation to frequency [33]. However, if the creation operator is applied before the field is switched on, meaning $t_2 < 0$, while the annihilation operator is applied after the field is turned on ($t_1 > 0$), the absolute value of $I(t_1, t_2)$ is given by

$$\begin{aligned}\left|I_{\text{sm}}^{t_2<0}(t_1, t_2)\right|^2 &= \left|-t_2 + \cos\left(\frac{E_0}{\Omega}\right) F_c(t_1, 0) + \sin\left(\frac{E_0}{\Omega}\right) F_s(t_1, 0)\right|^2 \\ &\quad + \left|\cos\left(\frac{E_0}{\Omega}\right) F_s(t_1, 0) - \sin\left(\frac{E_0}{\Omega}\right) F_c(t_1, 0)\right|^2 .\end{aligned}$$

Here F_c and F_s are the integrated functions $f_c(t)$ and $f_s(t)$ as defined in Eq. (3.21) and given by

$$F_c(t_1, t_2) = J_0\left(\frac{E_0}{\Omega}\right) t_{\text{rel}} + \phi_c(t_1) - \phi_c(t_2) \tag{3.32a}$$

$$F_s(t_1, t_2) = \phi_s(t_1) - \phi_s(t_2) . \tag{3.32b}$$

Finally, if the operator times obey $t_1 > t_2 > 0$, the absolute square of $I(t_1, t_2)$ yields

$$\begin{aligned}\left|I_{\text{sm}}^{t_2>0}(t_1, t_2)\right|^2 &= \left|\cos\left(\frac{E_0}{\Omega}\right) F_c(t_1, t_2) + \sin\left(\frac{E_0}{\Omega}\right) F_s(t_1, t_2)\right|^2 \\ &\quad + \left|\cos\left(\frac{E_0}{\Omega}\right) F_s(t_1, t_2) - \sin\left(\frac{E_0}{\Omega}\right) F_c(t_1, t_2)\right|^2 .\end{aligned}$$

For large average times the DOS of the system coupling to the semi-infinite sinusoidal driving should equal the DOS of an infinite sinusoidal driving, and by factoring the expression in Eq. (3.33) it can indeed be shown that it is equal to the expression in Eq. (3.24), i.e.

$$\left|I_{\text{sm}}^{t_2>0}(t_1, t_2)\right|^2 = \left[\cos^2\left(\frac{E_0}{\Omega}\right) + \sin^2\left(\frac{E_0}{\Omega}\right)\right] \times \left[F_c^2(t_1, t_2) + F_s^2(t_1, t_2)\right] \tag{3.33a}$$

$$= F_c^2(t_1, t_2) + F_s^2(t_1, t_2) \tag{3.33b}$$

$$= \left|I_\infty(t_1, t_2)\right|^2 . \tag{3.33c}$$

The function $F_c(t_1, t_2)$ is directly proportional to the Bessel function multiplied by t_{rel}. This means, that at large average times the relative time at which $t_2 = t_{\text{ave}} - (t_{\text{rel}}/2) < 0$ implies $\left|I_{\text{sm}}^{t_2>0}(t_1, t_2)\right|^2$ in Eq. (3.32) is so large that the Green function in Eq. (3.17) is essentially zero. In this case, it does not contribute to the DOS anymore.

This holds true as long as $F_c(t_1, t_2)$ is indeed increasing with t_{rel}, which is the case as long as the amplitude and the frequency of the driving are chosen in such a way that the Bessel function is not zero. However, if the Bessel function is zero, $\left|I_{\text{sm}}^{t_2>0}(t_1, t_2)\right|^2$ is not increasing for increasing relative times, while $\left|I_{\text{sm}}^{t_2<0}(t_1, t_2)\right|^2$ is still increasing because of the contribution of $-t_2$. This means that even for large average times, the Green function at $t_2 < 0$, i.e. $t_{\text{rel}} > 2t_{\text{ave}}$, contributes to the diagonal DOS, which will never be a set of delta functions and therefore never equal the DOS of the system coupled to an infinite drive.

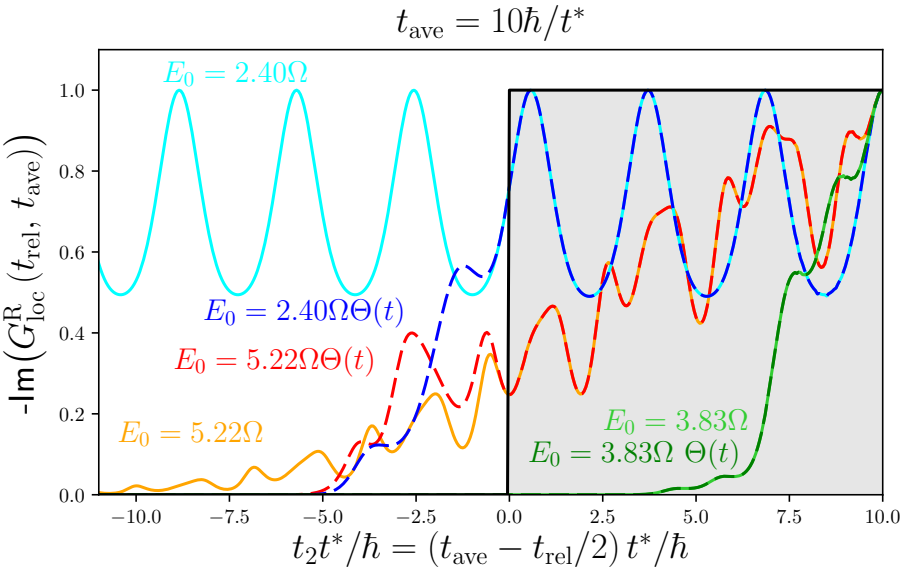

Figure 3.3: Negative imaginary part of the local Green function at $t_{\mathrm{ave}} = 10\hbar/t^*$, as a function of t_2 in units of inverse rescaled hopping $\hbar/t^*$ for different electric fields. Other parameters: $\Omega = t^*/\hbar$. Note that the real part vanishes because $\mu = 0$.

This scenario is displayed in Fig. 3.3. Here the imaginary part of the local, time-dependent Green function is plotted as a function of t_2 for fixed $t_{\mathrm{ave}} = 10\hbar/t^*$. Note that for retarded quantities $t_2 \leq t_{\mathrm{ave}}$ holds. The black line is the Heaviside step function, so the semi-infinite drive is turned on only in the area shaded in grey. The dashed lines correspond to the imaginary parts of the local, time-dependent Green functions of a semi-infinite drive, while the solid lines correspond to the infinite drive. Within the shaded box, the curves at the same amplitude E_0 match perfectly. But outside of that area, where $t_2 < 0$, the imaginary parts of the local, time-dependent Green functions corresponding to the semi-infinite drive decay faster than the functions corresponding to an infinite drive.

For the amplitude $E_0 = 3.83\Omega$, both the Green function for infinite drive (light green) and for semi-infinite drive (dark green) have completely decayed when $t_2 = 0$. This is because the magnitude of the Bessel function is large at $J_0\left(3.83\right) = -0.40$. In this case, choosing $t_{\mathrm{ave}} = 10\hbar/t^*$ is sufficient to interpret the DOS corresponding to the semi-infinite drive as a Floquet DOS. Contrary to that, the imaginary part of the local, time-dependent Green function with $E_0 = 5.22\Omega$ differs significantly from zero at $t_2 = 0$. This is because the magnitude of $J_0\left(5.22\right) = -0.10$ is small. For $t_2 < 0$ the function for semi-infinite drive (red) decays faster than for infinite drive (orange), so the DOS will not match due to these contributions from before $t = 0$ (when the semi-infinite drive is turned off). At this amplitude, only the DOS corresponding to larger average times can approximate the Floquet results. Finally, the local time dependent Green function corresponding to $E_0 = 2.40\Omega$ does not decay at all for the infinite drive (light blue). This is because $J_0\left(2.40\right) = 0$. However, for the semi-infinite drive (dark blue) it starts to decay immediately for $t_2 < 0$. This means the DOS corresponding to the infinite drive and the semi-infinite drive will never match, no matter how large the average time is chosen to be, and the DOS corresponding to semi-infinite

driving can never be interpreted as the Floquet DOS.

However, for the horizontal Fourier transformation the Green function only contributes to the horizontal DOS for $t > t_2$, which is why the horizontal DOS corresponding to the semi-infinite sinusoidal drive always equals the horizontal DOS corresponding to the infinite drive for all $t_2 > 0$ for any amplitude and frequency of the electric field.

3.4 Sinusoidal steplike pulse

A pulse that is turned on at t_0 and turned off after $n \in \mathbb{N}$ oscillations, i.e. at a cutoff time $t_\mathrm{c} = 2\pi n/\Omega$ is not experimentally implementable either, but there are experimental implementations that come close. One advantage of it is, that again the DOS can be computed analytically. Naturally, for $t_2 < t_1 < t_\mathrm{c}$ the DOS equals the results for semi-infinite driving, i.e. depending on the sign of t_2 the absolute value of $I(t_1, t_2)$ is given by Eq. (3.32) or Eq. (3.33). This also means that for the diagonal Fourier transform, the average time needs to be chosen large enough for the DOS corresponding to the semi-infinite driving to equal the DOS obtained by applying an infinite sinusoidal driving, as explained in section 3.3. However, for $0 < t_2 < t_\mathrm{c} < t_1$, the absolute value squared of $I(t_1, t_2)$ is given by

$$\begin{aligned}\left|I_\mathrm{sp}^{t_\mathrm{c}<t_1}(t_1, t_2)\right|^2 &= \left|t_1 - t_\mathrm{c} + \cos\left(\frac{E_0}{\Omega}\right) F_c(t_\mathrm{c}, t_2) + \sin\left(\frac{E_0}{\Omega}\right) F_s(t_\mathrm{c}, t_2)\right|^2 \\ &\quad + \left|\cos\left(\frac{E_0}{\Omega}\right) F_s(t_\mathrm{c}, t_2) - \sin\left(\frac{E_0}{\Omega}\right) F_c(t_\mathrm{c}, t_2)\right|^2,\end{aligned}$$

where the growing $t_1 - t_\mathrm{c}$ for increasing t_rel causes significant deviations from the DOS corresponding to infinite driving. Therefore, it is not enough to choose t_ave to be large and the Bessel function to have a finite size in order to interpret the results with Floquet theory, but also t_c must be large enough that the change in the local Green function that is caused by Eq. (3.34) has no further effect on the DOS. Similar to the semi-infinite driving, the dephasing in t_rel of the local retarded Green function is significantly faster if the Bessel function of the amplitude divided by the frequency of the electric field is large. Since the absolute value of $I(t_1, t_2)$ for $t_2 < 0$ and for $t_1 > t_\mathrm{c}$, given in Eq. (3.32) and Eq. (3.34) respectively, is eventually increasing for any electric field, while it is oscillating equally to the absolute value of $I(t_1, t_2)$ of the infinite sinusoidal driving for $0 < t_2 < t_1 < t_\mathrm{c}$ and $J_0(E_0/\Omega) = 0$, the DOS will never be a set of delta functions. The Green function for $t_1 > t_\mathrm{c}$ will eventually contribute to the DOS for both the horizontal and the diagonal Fourier transform, therefore at zeros of the Bessel function, the measured DOS corresponding to the sinusoidal steplike pulse can never be interpreted using Floquet theory, no matter which Fourier transform is chosen.

Studying the diagonal DOS for $0 < t_\mathrm{ave} < t_\mathrm{c}/2$, it is obvious that $t_2 < 0$ applies before $t_1 > t_\mathrm{c}$ needs to be taken into account, therefore here the results correspond to the results for the semi-infinite driving. However, for $t_\mathrm{c}/2 < t_\mathrm{ave} < t_\mathrm{c}$, the Green function at $t_\mathrm{c} < t_1$ needs to be considered before $t_2 < 0$ applies. Therefore, for Floquet theory to be valid, the Green function has to be approximately zero at $t_1 = t_c$ in order for it to have a negligible contribution to the DOS. Because the dephasing in t_rel in the local Green function is faster

the larger the value of the Bessel function multiplied by $\sin(E_0/\Omega)$ and $\cos(E_0/\Omega)$ is, the cutoff time t_c can be chosen significantly smaller for large values of the Bessel functions.

Note that it is most suitable to set the average time to $t_{\mathrm{ave}} = t_{\mathrm{c}}/2$ because in this case $t_2 = 0$ and $t_1 = t_c$ occur at the same relative time $t_{\mathrm{rel}} = t_{\mathrm{c}}$. When t_{ave} is chosen to be the minimal average time $t_{\mathrm{ave}}^{\mathrm{min}}$ at which the DOS corresponding to a semi-infinite drive equals the DOS for infinite driving, then $t_{\mathrm{c}} = 2t_{\mathrm{ave}}^{\mathrm{min}}$ is the shortest cutoff time at which the DOS of the steplike pulse can be interpreted with Floquet theory.

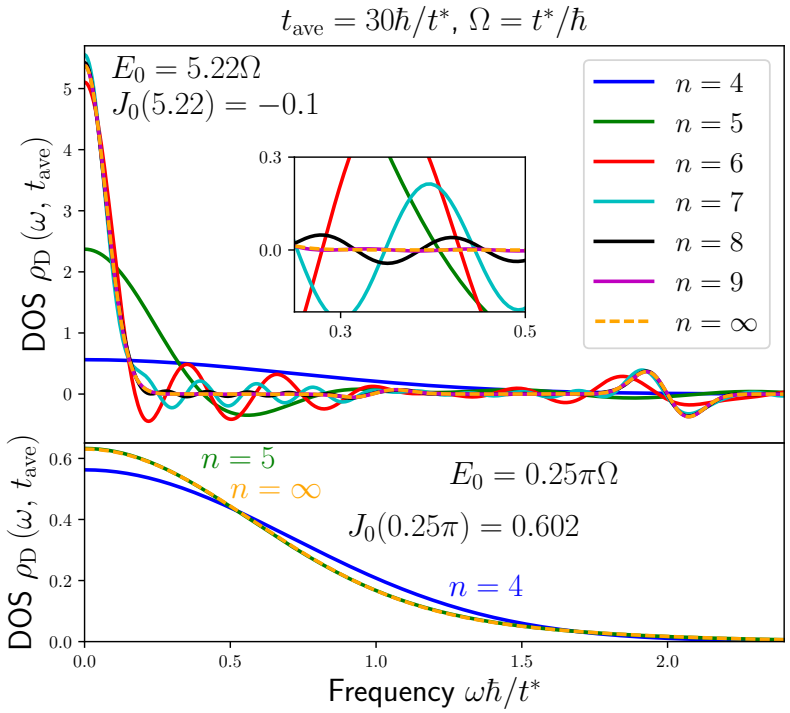

Figure 3.4: The diagonal DOS corresponding to the steplike pulse that starts at $t = 0$ and is turned off after n oscillations at a cutoff time $t_{\mathrm{c}} = 2\pi n/\Omega$ and corresponding to an infinite sinusoidal drive for $\Omega = t^*/\hbar$, $t_{\mathrm{ave}} = 30\hbar/t^*$ and two different amplitudes $E_0 = 5.22\Omega$ (upper panel) and $E_0 = \pi\Omega/4$ (lower panel).

Figure 3.4 displays the diagonal DOS corresponding to the steplike pulse and to infinite sinusoidal driving for $\Omega = t^*/\hbar$ at two different amplitudes of the electric field. The average time is chosen to be $t_{\mathrm{ave}} = 30\hbar/t^*$ because earlier analyses have shown that this is sufficiently large for the diagonal DOS of the semi-infinite sinusoidal drive to equal the DOS associated with infinite driving. For $t_c < t_{\mathrm{ave}}$, the squared absolute value of $I(t_1, t_2)$ is given by $|t_{\mathrm{rel}}|^2$, so for $t_2 < t_1 < 0$, the local retarded Green function (and therefore the DOS) are Gaussian and equal to the noninteracting DOS, as explained in section 3.3. This is why the blue line at $n = 4$, i.e. at $t_{\mathrm{c}} = 4 \cdot 2\pi\hbar/t^* < t_{\mathrm{ave}} = 30\hbar/t^*$, is Gaussian and the same for both amplitudes of the electric field.

In the upper panel of Fig. 3.4, the amplitude of the electric field is given by $E_0 = 5.22\Omega$, so that the magnitude of the Bessel function is small $[J_0(5.22) = -0.10]$. This means the

dephasing in t_{rel} is slow (as can be seen in Fig. 3.2), so t_c has to be chosen quite large in order for Floquet theory to be applicable. When contemplating the DOS at $n \in \{5, 6, 7\}$ in the upper panel, it is obvious that it is completely different from the DOS of the infinite sinusoidal pulse, which is displayed in orange. Only at $n = 8$ do we start to see some similarity, and the lines seem to match at $n = 9$. However, only $n = 10$ (this is not displayed, as the deviations from $n = 9$ are too small to be seen) is sufficient for the two diagonal DOS to be essentially equal. This means t_c needs to be chosen to be twice as large as t_{ave} when the results are meant to be interpreted with Floquet theory.

In the lower panel of Fig. 3.4, the amplitude of the electric field is chosen to be $E_0 = 0.25\pi\Omega$. In this case, the magnitude of $J_0(0.25\pi) = 0.602$ is large and both $\cos(0.25\pi) = \sin(0.25\pi) = 1/\sqrt{2}$ are large too. Contrary to the DOS corresponding to a small value of the Bessel function, we find that the Gaussian diagonal DOS at $t_{\mathrm{ave}} > t_{\mathrm{c}}$ ($n = 4$, blue), shows similarities to the diagonal DOS corresponding to the infinite sinusoidal driving. Furthermore, as soon as $t_{\mathrm{ave}} < t_{\mathrm{c}}$ ($n = 5$, green), the DOS are equal. Note that the average time in the lower panel is chosen to be $t_{\mathrm{ave}} = 30\hbar/t^*$ to ensure comparability with the upper panel. But while $t_{\mathrm{ave}} = 30\hbar/t^* \approx t_{\mathrm{ave}}^{\mathrm{min}}$ holds for $E_0 = 5.22\Omega$ (upper panel), the minimal average time for $E_0 = 0.25\pi\Omega$ is much smaller at $t_{\mathrm{ave}}^{\mathrm{min}} \ll t_{\mathrm{ave}} = 30\hbar/t^*$. Therefore, in the lower panel, $t_{\mathrm{c}} \ll 2t_{\mathrm{ave}}$ is sufficient to interpret the DOS with Floquet theory.

The observations above hold for the horizontal DOS as well, the major difference being that t_{ave} does not need to be chosen as large. In fact, in this case, choosing $t_{\mathrm{ave}} = 0$ is ideal, as only the magnitude of $t_{\mathrm{c}} - t_{\mathrm{ave}}$ determines the quality of the results for a given electric field.

3.5 Sinusoidal Gaussian pulse

A field pump that is implementable in an experiment is a sinusoidal electric field that is modulated with a Gaussian envelope, i.e. an electric field that is given by

$$E(t) = E\sin(\Omega t)\exp\left[-\left(\frac{t}{t_{\mathrm{E}}}\right)^2\right] \tag{3.34a}$$

$$= -\frac{iE}{2}\exp\left[-\left(\frac{\Omega t_{\mathrm{E}}}{2}\right)^2\right]\left(\exp\left[\left(\frac{\Omega t_{\mathrm{E}}}{2} + i\frac{t}{t_{\mathrm{E}}}\right)^2\right] - \exp\left[\left(\frac{\Omega t_{\mathrm{E}}}{2} - i\frac{t}{t_{\mathrm{E}}}\right)^2\right]\right), \tag{3.34b}$$

where t_{E} is the width of the Gaussian. The vector potential A_{G} corresponding to the field in Eq. (3.34a) can be computed using the imaginary error function

$$\mathrm{erfi}(a + ibx) = \frac{2bi}{\sqrt{\pi}}\int_0^x \exp\left[(a + ubi)^2\right]\,\mathrm{d}u \qquad a, b \in \mathbb{R}, \tag{3.35}$$

which obeys

$$\mathrm{erfi}(a + ibx) + \mathrm{erfi}(a - ibx) = 2\mathrm{Re}\left[\mathrm{erfi}(a + ibx)\right]. \tag{3.36}$$

It is given by

$$A_{\mathrm{G}}(t) = \frac{cEt_{\mathrm{E}}\sqrt{\pi}}{2} e^{-\left(\frac{\Omega t_{\mathrm{E}}}{2}\right)^2} \mathrm{Re}\left[\mathrm{erfi}\left(\frac{\Omega t_{\mathrm{E}}}{2} + \frac{it}{t_{\mathrm{E}}}\right)\right] . \tag{3.37}$$

Using the Faddeeva function

$$\mathrm{w}(z) = e^{-z}\left(1 + i\mathrm{erfi}(z)\right) , \tag{3.38}$$

this vector potential can also be expressed as

$$A_{\mathrm{G}}(t) = \frac{cEt_{\mathrm{E}}\sqrt{\pi}}{2} e^{-\left(\frac{t}{t_{\mathrm{E}}}\right)^2} \mathrm{Im}\left[\mathrm{w}\left(\frac{\Omega t_{\mathrm{E}}}{2} + \frac{it}{t_{\mathrm{E}}}\right) e^{i\Omega t}\right] , \tag{3.39}$$

and it shares many properties with the vector potential for the infinite sinusoidal pulse in Eq. (3.19). Both vector potentials have the same zeros and oscillate with the same frequency, the major difference is the decaying amplitude for the oscillations in the vector potential A_{G}. Since we are not able to calculate an analytic form for the local retarded Green function from that, we simply calculate it numerically. What we find is that as the Gaussian broadens, the corresponding DOS does not simply approach the DOS of an infinite sinusoidal drive, but oscillates around it (see Fig. 3.5b). It requires a second averaging, more precisely a running average over one period of these oscillations in ω, for the DOS of the Gaussian pulse to match the DOS of the infinite sinusoidal driving.

This can be traced back to an additional peak in the imaginary part of the time-dependent local Green function, whose position and shape are functions of the amplitude E_0, the frequency Ω and the width t_{E} of a pulse (see Fig. 3.5a). Figure 3.5a shows that for a wide Gaussian, the imaginary part of the time-dependent local Green function perfectly matches the imaginary part of the time-dependent local Green function of the system coupling to an infinite drive up to a relative time at which the Green function of the infinite drive completely decays. The Green function of the Gaussian pulse has a single complex revival at a later relative time.

The amplitude of the electric field is chosen to be $E_0 = 3.83\Omega$ so the Bessel function of the amplitude divided by the frequency is at its first minimum. This ensures a fast decay of the Green function corresponding to the infinite sinusoidal drive as explained in Sect. 3.2. Therefore, this amplitude leads to the best agreement between the Green function corresponding to an infinite drive (orange) and the Green function of the pulsed systems (blue and green) before the latter Green functions have their revival.

This behavior is illustrated further in Fig. 3.5b, which displays the diagonal DOS corresponding to an infinite sinusoidal drive (blue) and a pulsed system (green) in frequency space. Both diagonal DOS are averaged over the Floquet period from $t_{\mathrm{ave}} = -\pi/\Omega$ to $t_{\mathrm{ave}} = \pi/\Omega$, evenly around the center of the pulse. Any averaging that is not centered around the pulse leads to significantly worse results. The orange line in Fig. 3.5b is the running average in frequency ω over one period of the oscillations in the diagonal DOS of the pulsed system, i.e., the average over one period of the oscillations of the green line.

For an amplitude at which the Bessel Function $J_0(E_0/\Omega)$ is small ($E_0 = 5.22\Omega$, upper panel in Fig. 3.5b), the diagonal DOS of the pulsed system shows large deviations from the

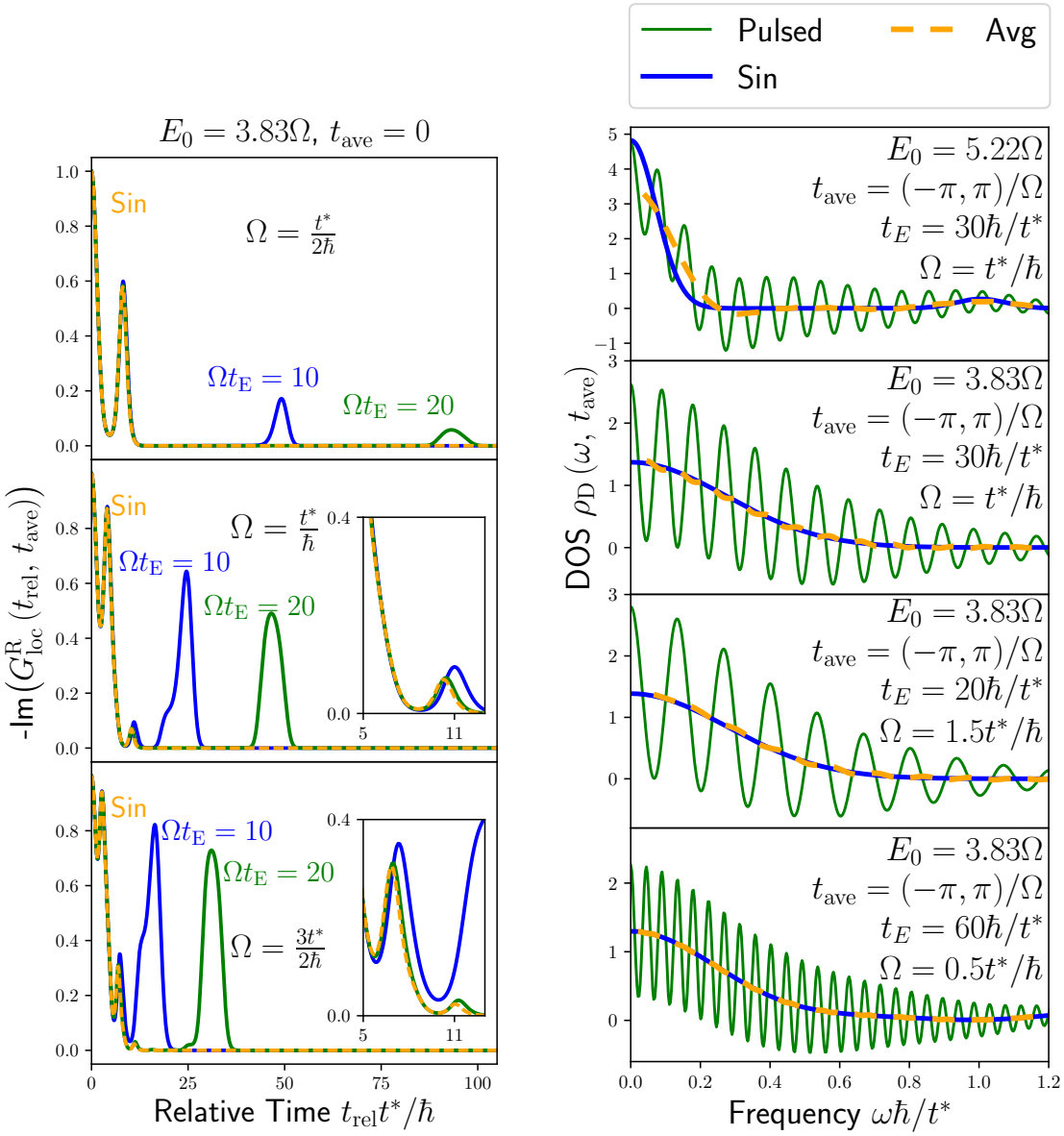

(a) Negative imaginary part of the local Green function at a constant average time $t_{\text{ave}} = 0$, as a function of t_{rel} in units of inverse rescaled hopping $\hbar/t^*$ at $E_0 = 3.83\Omega$ for an infinite sinusoidal drive (orange) and for two Gaussians where the product of the width of the Gaussian and the frequency of the electric field is $\Omega t_{\text{E}} = 10$ (blue) and $\Omega t_{\text{E}} = 20$ (green) respectively, at three different driving frequencies $\Omega = 0.5t^*/\hbar$ (upper panel), $\Omega = t^*/\hbar$ (middle panel) and $\Omega = 1.5t^*/\hbar$ (lower panel).

(b) The diagonal DOS corresponding to an infinite sinusoidal drive (blue) and a system that is exposed to a sinusoidal driving with a Gaussian envelope (green), both averaged over the Floquet period from $t_{\text{ave}} = -\pi/\Omega$ to $t_{\text{ave}} = \pi/\Omega$ and the running average in the frequency ω (orange) over one period of the oscillations in the diagonal DOS of the pulsed system at different amplitudes and frequencies of the electric field and for a Gaussian pulse of varying width.

Figure 3.5: Negative imaginary part of the local Green function and diagonal DOS for a sinusoidal Gaussian pulse and variing parameters Ω, t_{E} and t_{ave}.

diagonal DOS corresponding to the infinite sinusoidal drive even after taking the running average (especially for small frequencies ω). However, at $E_0 = 3.83\Omega$ (first minimum of the Bessel function, second panel in Fig. 3.5b), the agreement between the diagonal DOS of the system coupling to an infinite sinusoidal drive and the running average over the diagonal DOS of the pulsed system is good (all parameters except for E_0 are the same in the two upper panels).

To explain the connection between the frequency of the oscillations in the DOS and both the width of the Gaussian t_E and the frequency Ω of the electric field, it is useful to study the imaginary part of the local time dependent Green function (see Fig. 3.5a). For a wider Gaussian, i.e., larger t_E (for fixed Ω) the revival occurs later, meaning that the oscillations in the DOS show a higher frequency. In fact, the time at which the revival occurs seems to be almost linearly connected to the width of the Gaussian, as a shift by some factor α in the width $t_\mathrm{E} \to \alpha t_\mathrm{E}$ leads to the revival time shifting from t_rel to αt_rel. Varying Ω on the other hand has little effect on the relative time at which the revival occurs, but for a constant pulse width t_E the agreement between the Green function of the infinitely driven system and the Green function of the pulsed system diminishes for very small Ω. Another disadvantage of low frequencies is that the Fourier period $2\pi/\Omega$ increases, so when calculating the averaged DOS the Green function requires contributions from average times that are much further away from the center of the pulse.

Figure 3.5a shows that at any given frequency Ω, the revival occurs later whenever the product Ωt_E is larger. That is, the green peak for $\Omega t_\mathrm{E} = 20$ always occurs at a later relative time than the blue peak at $\Omega t_\mathrm{E} = 10$. The agreement between the running average of the DOS of the pumped system and the DOS of the system coupling to an infinite drive is generally better for later times of the revival in the Green function. This is because for early arrival times, the Green function corresponding to the infinite drive may not have completely decayed when the revival occurs. That is, the resemblance between the two DOS is better at high frequencies Ω and for broad Gaussian pulses. This is not surprising, as it means that the pumped field resembles the infinite sinusoidal field when it has a larger amount of oscillations. Therefore it is more interesting to compare the Green functions and the resulting DOS at varying frequencies Ω where the product Ωt_E of the width of the pulse and the frequency of the electric field is kept constant.

By comparing the revival times at the frequencies $\Omega = 0.5t^*/\hbar$, $\Omega = t^*/\hbar$ and $\Omega = 1.5t^*/\hbar$ (with Ωt_E fixed) in Fig. 3.5a, it is clear that the revival occurs later for lower frequencies. This directly results from the later occurrence of the revival as the Gaussian broadens. At $\Omega = 0.5t^*/\hbar$ (upper panel of Fig. 3.5a), the revivals of both $\Omega t_\mathrm{E} = 10$ and $\Omega t_\mathrm{E} = 20$ occur long after the Green function corresponding to the infinite drive has decayed. This means that the agreement between the curves is good up to this point. But this agreement becomes worse at larger frequencies. For $\Omega = t^*/\hbar$ (middle panel in Fig. 3.5a) the green curve at $\Omega t_\mathrm{E} = 20$ still matches the Green function of the system coupling to an infinite drive up to the point where the latter one has decayed, but the revival of the blue curve at $\Omega t_\mathrm{E} = 10$ moves to times t_rel where the Green function corresponding to the infinite drive has not completely decayed. The deviations before the decay of the Green function become even larger at higher frequencies like $\Omega = 1.5t^*/\hbar$ (lower panel in Fig. 3.5a). This implies that the applicability of Floquet theory is strongly dependent on the width of the Gaussian, and

to a lesser extent on the driving frequency Ω. A wide Gaussian ensures that the measured DOS resembles the DOS of the infinitely driven system, even if the frequency of the driving field is low.

Figure 3.5b confirms these conclusions. Comparing the lower three panels, where the width of the Gaussian and the frequency of the electric field are chosen so $\Omega t_{\mathrm{E}} = 30$ holds, it becomes clear that the frequency with which the diagonal DOS of the pulsed system oscillates around the DOS corresponding to the infinite drive is increasing as the Gaussian broadens and the frequency of the driving field decreases. Note that even though the diagonal DOS of the pulsed system (green) is averaged over the Floquet period, the oscillations take negative values, i.e. the averaged DOS is not semidefinite even if the Gaussian is broad. As explained in Sect. 3.2, it is required for the DOS averaged over the Floquet period to be semidefinite if we want the pulsed system to be representative of the Floquet results. Fortunately, the orange line that results from calculating the running average over one period of the oscillations in the DOS (corresponding to the Gaussian pulse) is semidefinite and resembles the DOS of the infinitely driven system well.

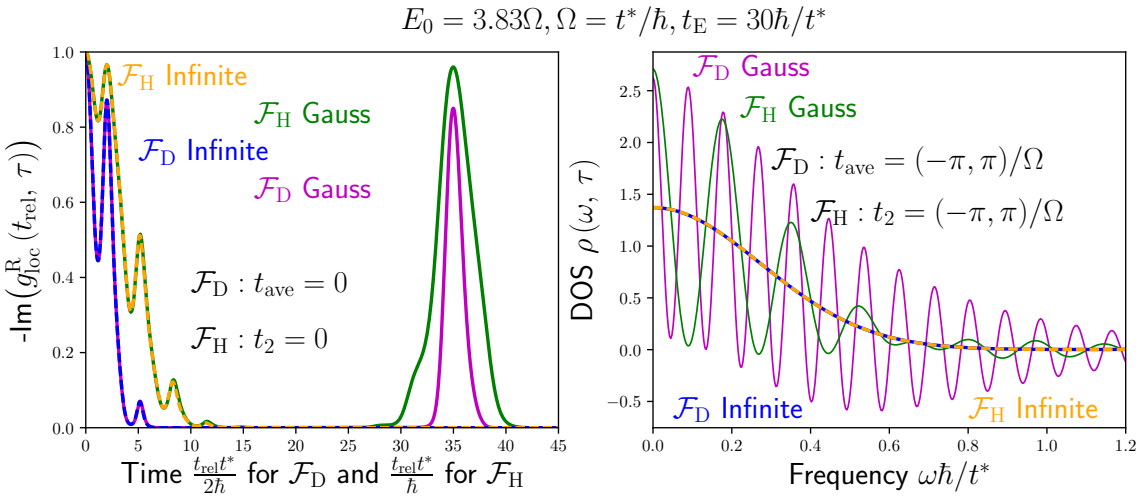

Figure 3.6: The left panel: Green function of both the pulsed system (labeled "Gauss") and the system that is driven for an infinitely long time (labeled "Infinite") for a constant $t_2 = 0$ ($\mathcal{F}_{\mathrm{H}}$) and a constant $t_{\mathrm{ave}} = 0$ ($\mathcal{F}_{\mathrm{D}}$). Right panel: horizontal and diagonal DOS of both systems, averaged over one Fourier period in t_2 and t_{ave} respectively. Other parameters: $E_0 = 3.83\Omega$, $\Omega = t^*/\hbar$ and $t_{\mathrm{E}} = 30\hbar/t^*$.

The results for the horizontal Fourier transformation are similar to the results obtained using the diagonal Fourier transformation. The major difference is a factor of 2 in the relative time that was already mentioned in Sec. 3.2 and is caused by the relation $t_1 = t_{\mathrm{ave}} + t_{\mathrm{rel}}/2$. The left panel in Fig. 3.6 shows the Green function of both the pulsed system and the system that is driven for an infinitely long time at $E_0 = 3.83\Omega$, $\Omega = t^*/\hbar$ and $t_{\mathrm{E}} = 30\hbar/t^*$, both for $t_{\mathrm{ave}} = 0$ and for $t_2 = 0$. Note that the Green functions are given in terms of $t_{\mathrm{rel}}/2$ for the constant average time $t_{\mathrm{ave}} = 0$ (magenta) and in terms of t_{rel} for a constant $t_2 = 0$ (green). This is to emphasize the fact that the peak of the revival in the Green function corresponding to a constant t_2 takes place at exactly half of the relative time at which the

peak of the revival in the Green function corresponding to a constant t_{ave} is located. In fact, for small relative times, even the relative times at which the Green functions of the system that is coupling to an infinite drive (orange and blue) go through extrema are separated by this factor 2.

The right panel of Fig. 3.6 displays the diagonal and the horizontal DOS of the pulsed system and the infinitely driven system, both averaged over one Fourier period from $t_{\text{ave}} = -\pi/\Omega$ to $t_{\text{ave}} = \pi/\Omega$ for constant t_{ave} and from $t_2 = -\pi/\Omega$ to $t_2 = \pi/\Omega$ for constant t_2. Note that this averaging leads to exactly the same DOS for the infinite drive (blue and orange), no matter which Fourier transform is computed (as shown in Sec. 3.2). The diagonal DOS (magenta) of the pulsed system, however, oscillates with almost double the frequency of the horizontal DOS (green) of the same system. While the period of the oscillations in the horizontal DOS is almost perfectly constant and the amplitude of these oscillations decreases monotonically, the period of the oscillations of the horizontal DOS varies significantly more. Though the amplitude of the horizontal DOS shows an overall decay, it does not decrease monotonically. This leads to a slightly worse agreement between the DOS corresponding to the infinite drive and the running average over one period of the oscillations in the DOS for the Gaussian pulse when the DOS is horizontal.

Note that the second "revival" peak of the time dependent local Green function is expected to be smaller for interacting systems where Green functions decay more rapidly in imaginary time. So these oscillations may be reduced when interactions are included.

4 Periodically driven, interacting systems

In section 3.2 we found proof that conventional definition of the instantaneous DOS as the imaginary part of the retarded local Green function evaluated at fixed t_{ave} is not positive semi-definite. But the time-averaged density of states always is. In this chapter we will generalize these results for periodically driven, interacting systems, which allows us to draw general conclusions about spectral functions, their sum rules and the Dyson equation. To distinguish between a spectral function that is not necessarily positive-semidefinite and a spectral function that can indeed be interpreted as a DOS we will generally refer to the function defined by $\rho(\omega, t_{\text{ave}}) := -\pi^{-1}\text{Im}G(\omega, t_{\text{ave}})$ as *spectral function* and only call it *DOS* when we can proof that it is nonnegative and can hence be interpreted as a DOS as in equilibrium.

4.1 Positivity of the spectral densities of retarded Floquet Green functions

When studying the spectral functions of a periodically driven, interacting system, it is useful to first to recall the Lehmann representation for a constant Hamiltonian $\mathcal{H}$. Let us assume that $\{|m\rangle\}$ is an eigen basis of $\mathcal{H}$ with eigen values ϵ_m and that the system is in the state $|m\rangle$ with probability $p_m \geq 0$ and $\sum_m p_m = 1$. We do not necessarily require a thermal distribution $p_m \propto \exp(-\beta\epsilon_m)$, but we do require monotonicity for the bosonic case, where $p_m \geq p_n$ if $\epsilon_m \leq \epsilon_n$. For a Hamiltonian that is constant in time, the probability p_m is given by

$$p_m = \frac{1}{Z} e^{-\beta\epsilon_n} \tag{4.1}$$

with the partition function $Z = \text{Tr}e^{-\beta\mathcal{H}}$ [45]. In this case, the greater Green function (2.2a) is given by

$$G^{>}(t_1, t_2) := -i \left\langle c(t_1)c^\dagger(t_2)\right\rangle \tag{4.2a}$$

$$= -i \sum_m p_m \left\langle m\right| c(t_1)c^\dagger(t_2) \left|m\right\rangle \ . \tag{4.2b}$$

At this point, it is useful to switch from the Heisenberg picture, where the operators depend on time and contain the information that is necessary to describe the system, to the Schrödinger picture, where the evolution of the system is contained in the state vectors. The transformation from the Heisenberg to the Schrödinger picture for operators that have no explicit time dependence in the Schrödinger picture is given by

$$c_{\text{H}}(t) = U^\dagger(t, t_0)\, c_{\text{S}} U(t, t_0) \ . \tag{4.3}$$

To simplify notation, we will suppress the time dependence in the following calculations, and simply write $c(t)$ for an operator in the Heisenberg picture and c for an operator in the Schrödinger picture. The time evolution operator for a Hamiltonian that is constant in time is given by

$$U(t,t_0) = \exp\left[-i\mathcal{H}\,(t-t_0)\right]\,. \tag{4.4}$$

It is easy to see that $U^\dagger(t,t_0) = U(t_0,t)$, so the greater Green function is given by

$$\begin{aligned} G^>(t_1,t_2) =& -i\sum_m p_m \langle m|\, U(t_0,t_1)\, cU(t_1,t_0)\, U(t_0,t_2)\, c^\dagger U(t,t_0)\,|m\rangle & \text{(4.5a)}\\ =& -i\sum_m p_m \langle m|\, e^{i\mathcal{H}(t_1-t_0)} c e^{-i\mathcal{H}t_1} e^{i\mathcal{H}t_2} c^\dagger e^{-i\mathcal{H}(t_2-t_0)}\,|m\rangle\,. & \text{(4.5b)}\end{aligned}$$

At this point we can use that $\{|m\rangle\}$ is an eigen basis of $\mathcal{H}$, so

$$e^{-i\mathcal{H}t}\,|m\rangle = |m\rangle\, e^{-i\epsilon_m t} \tag{4.6}$$

holds, and we get

$$\begin{aligned} G^>(t_1,t_2) =& -i\sum_m p_m \langle m|\, U(t_0,t_1)\, cU(t_1,t_0)\, U(t_0,t_2)\, c^\dagger U(t,t_0)\,|m\rangle & \text{(4.7a)}\\ =& -i\sum_{m,n} p_m e^{i\epsilon_m t_1}\,\langle m|\, c\,|n\rangle\, e^{-i\epsilon_n t_1} e^{i\epsilon_n t_2}\,\langle n|\, c^\dagger\,|m\rangle\, e^{-i\epsilon_m t_2} & \text{(4.7b)}\\ =& -i\sum_{m,n} p_m e^{i(\epsilon_m-\epsilon_n)t_{\mathrm{rel}}}\,|\langle m|\, c\,|n\rangle|^2\,. & \text{(4.7c)}\end{aligned}$$

This obviously only depends on the relative time. The same holds for both the lesser Green function, which yields

$$\begin{aligned} G^<(t_1,t_2) :=& \pm i\,\langle c^\dagger(t_2)c(t_1)\rangle & \text{(4.8)}\\ =& \pm i\sum_{m,n} p_n e^{i(\epsilon_m-\epsilon_n)t_{\mathrm{rel}}}\,|\langle m|\, c\,|n\rangle|^2 & \text{(4.9)}\end{aligned}$$

and the retarded Green function, which is given by

$$G^{\mathrm{R}}(t_{\mathrm{rel}}) = -i\sum_{m,n}(p_m \pm p_n)\, e^{i(\epsilon_m-\epsilon_n)t_{\mathrm{rel}}}\,|\langle m|\, c\,|n\rangle|^2\,\Theta(t_{\mathrm{rel}})\,, \tag{4.10}$$

and where the $+$ refers to fermionic operators and the $-$ to bosonic ones. The frequency dependent response yields

$$\begin{aligned} G^{\mathrm{R}}(\omega) =& -i\sum_{m,n}(p_m \pm p_n)\,|\langle m|\, c\,|n\rangle|^2 \lim_{\delta\to 0+}\int_0^\infty e^{i(\omega+i\delta+\epsilon_m-\epsilon_n)t_{\mathrm{rel}}}dt_{\mathrm{rel}} & \text{(4.11a)}\\ =& -i\sum_{m,n}(p_m \pm p_n)\,|\langle m|\, c\,|n\rangle|^2\left\{\pi\delta(\omega+\epsilon_m-\epsilon_n) + iP\left[\frac{1}{\omega+\epsilon_m-\epsilon_n}\right]\right\}\,, & \text{(4.11b)}\end{aligned}$$

where P stands for the principle value of the pole. The spectral function is hence given by

$$\begin{aligned} \rho(\omega) =& -\frac{1}{\pi}\mathrm{Im}\left[G^{\mathrm{R}}(\omega)\right] & \text{(4.12a)}\\ =& \sum_{m,n}(p_m \pm p_n)\,|\langle m|\, c\,|n\rangle|^2\,\delta(\omega+\epsilon_m-\epsilon_n)\,, & \text{(4.12b)}\end{aligned}$$

which does not depend on t_{ave} because $\mathcal{H}$ is constant. Recall that $\rho(\omega)$ is strictly nonnegative in the fermionic case and in the bosonic case for $\omega \geq 0$ since $\epsilon_n \geq \epsilon_m$ implies $p_n \leq p_m$; for bosons and $\omega \leq 0$ $\rho(\omega)$ is nonpositive.

If the Hamiltonian is not constant but periodic in time, the situation is more complicated, because of the time dependence of the Floquet state solutions $|m,t\rangle$ given in Eq. (2.12). We assume that the system was at some time t_0 in the Floquet state $|m,t_0\rangle$ with probability p_m, so the greater Green function we have to consider here is given by

$$G^{>}(t_1,t_2) = -i \sum_{m=0}^{\infty} p_m \langle m,t_0| \, c(t_1) c^{\dagger}(t_2) \, |m,t_0\rangle \, . \tag{4.13}$$

Inserting the time evolution operator

$$U(t_1,t_2) = \sum_m \exp(-i\epsilon_m(t_1-t_2)) \; |m,t_1\rangle \langle m,t_2| \tag{4.14}$$

we derived in section 2.2 yields

$$G^{>}(t_1,t_2) = -i \sum_{m=0}^{\infty} p_m \langle m,t_0| \, U(t_0,t_1) \, c \, U(t_1,t_2) c^{\dagger} \, U(t_2,t_0) \, |m,t_0\rangle \tag{4.15}$$

$$= -i \sum_{m,n=0}^{\infty} p_m e^{-i\epsilon_m(t_0-t_1)} \langle m,t_1| \, c \, |n,t_1\rangle \, e^{-i\epsilon_n(t_1-t_2)} \langle n,t_2| \, c^{\dagger} \, |m,t_2\rangle \, e^{-i\epsilon_m(t_2-t_0)}. \tag{4.16}$$

$$= -i \sum_{m,n=0}^{\infty} p_m e^{i(\epsilon_m-\epsilon_n)t_{\text{rel}}} \langle m,t_1| \, c \, |n,t_1\rangle \langle n,t_2| \, c^{\dagger} \, |m,t_2\rangle \; . \tag{4.17}$$

Obviously the dependence on t_0 cancels out so that one may choose any appropriate instant. From this point, the proof of the nonnegativity of the averaged spectral function for periodically driven, interacting systems closely resembles the proof for the periodically driven, noninteracting system in infinite dimensions, that we gave in section 3.2. We define the T-periodic functions

$$\Phi_{m,n}(t) := \langle m,t| \, c \, |n,t\rangle \tag{4.18}$$

that generalize the T-periodic functions in Eq. (3.27), by including the Floquet incices m and n. Eq. (4.18) directly implies

$$\Phi^*_{m,n}(t) := \langle n,t| \, c^{\dagger} \, |m,t\rangle \tag{4.19}$$

so that we can express (4.17) by

$$G^{>}(t_1,t_2) = -i \sum_{m,n=0}^{\infty} p_m e^{i(\epsilon_m-\epsilon_n)t_{\text{rel}}} \Phi_{m,n}(t_1) \Phi^*_{m,n}(t_2). \tag{4.20}$$

Analog to the lesser Green function in (4.20), the greater Green function can be expressed as

$$G^{<}(t_1,t_2) = \pm i \sum_{m,n=0}^{\infty} p_n e^{i(\epsilon_m-\epsilon_n)t_{\text{rel}}} \Phi_{m,n}(t_1) \Phi^*_{m,n}(t_2). \tag{4.21}$$

yielding the retarded Green function

$$G^{\mathrm{R}}(t_1,t_2) = G^{>}(t_1,t_2) - G^{<}(t_1,t_2)\Theta(t_1-t_2) \tag{4.22a}$$

$$= -i\sum_{m,n=0}^{\infty}\left(p_m \pm p_n\right) e^{i(\epsilon_m-\epsilon_n)t_{\mathrm{rel}}}\Phi_{m,n}(t_1)\Phi^{*}_{m,n}(t_2)\Theta(t_1-t_2). \tag{4.22b}$$

This result strongly resembles (4.10), but cannot be Fourier transformed directly due to the time dependence of $\Phi_{m,n}(t)$. But the latter can be represented by its Fourier series due to its periodicity

$$\Phi_{m,n}(t) = \sum_{\alpha\in\mathbb{Z}} f^{(\alpha)}_{m,n} e^{i\alpha\Omega t} \tag{4.23a}$$

$$\Phi^{*}_{m,n}(t) = \sum_{\alpha\in\mathbb{Z}} \left(f^{(\alpha)}_{m,n}\right)^{*} e^{-i\alpha\Omega t}\,, \tag{4.23b}$$

where $\Omega = 2\pi/T$.

The Wigner representation [37] of the retarded Green function is defined to be

$$G_\ell(\omega) = \int_{\infty}^{\infty} dt_{\mathrm{rel}} e^{i\omega t_{\mathrm{rel}}} \frac{1}{T}\int_{-\frac{T}{2}}^{\frac{T}{2}} dt_{\mathrm{ave}} e^{i\ell\Omega t_{\mathrm{ave}}} G^{\mathrm{R}}(t_1,t_2). \tag{4.24}$$

The physical interpretation of the Wigner representation is, that G_ℓ is the ℓ^{th} oscillating mode in t_{ave} of $G_\ell(t_1,t_2)$ [25]. To calculate the Wigner representation of Eq. (4.22b), we first compute the integral over the average time, given by

$$\frac{1}{T}\int_{-\frac{T}{2}}^{\frac{T}{2}} dt_{\mathrm{ave}} e^{i\ell\Omega t_{\mathrm{ave}}} \Phi_{m,n}\left(t_{\mathrm{ave}} + \frac{t_{\mathrm{rel}}}{2}\right)\Phi^{*}_{m,n}\left(t_{\mathrm{ave}} - \frac{t_{\mathrm{rel}}}{2}\right) = \sum_{\alpha} f^{(\alpha)}_{m,n}\left(f^{(\alpha+\ell)}_{m,n}\right)^{*} e^{i\Omega t_{\mathrm{rel}}(\alpha+\frac{\ell}{2})}\,. \tag{4.25}$$

This leads to the Wigner representation

$$G_\ell(\omega) = -i\sum_{m,n=0}^{\infty}\left(p_m \pm p_n\right)\sum_{\alpha} f^{(\alpha)}_{m,n}\left(f^{(\alpha+\ell)}_{m,n}\right)^{*}\int_{-\infty}^{\infty} dt_{\mathrm{rel}}\Theta(t_{\mathrm{rel}}) e^{i\omega t_{\mathrm{rel}}} e^{i(\epsilon_m-\epsilon_n)t_{\mathrm{rel}}} e^{i\Omega t_{\mathrm{rel}}(\alpha+\frac{\ell}{2})} \tag{4.26a}$$

$$= -i\sum_{m,n=0}^{\infty}\left(p_m \pm p_n\right)\sum_{\alpha} f^{(\alpha)}_{m,n}\left(f^{(\alpha+\ell)}_{m,n}\right)^{*}\lim_{\Delta\to 0+}\int_{0}^{\infty} dt_{\mathrm{rel}} e^{it_{\mathrm{rel}}(\epsilon_m-\epsilon_n+\Omega(\alpha+\frac{\ell}{2})+\omega+i\Delta)} \tag{4.26b}$$

$$= -i\sum_{m,n=0}^{\infty}\left(p_m \pm p_n\right)\sum_{\alpha} f^{(\alpha)}_{m,n}\left(f^{(\alpha+\ell)}_{m,n}\right)^{*}\times\left\{\pi\delta\left(\Delta\epsilon\right) + i\mathrm{P}\left[\frac{1}{\Delta\epsilon}\right]\right\}. \tag{4.26c}$$

In Eq. (4.26c) we defined

$$\Delta\epsilon := \omega - (\epsilon_n - \epsilon_m) + (\alpha+\ell/2)\,\Omega\,. \tag{4.27}$$

At this point we can obtain the Fourier coefficients

$$\rho(\omega, t_{\mathrm{ave}}) = \sum_{\alpha\in\mathbb{Z}} A_\ell(\omega)\exp(-i\ell\Omega t_{\mathrm{ave}}) \tag{4.28}$$

of the Fourier series of the retarded spectral function:

$$\rho_\ell(\omega) = -\frac{1}{\pi}\mathrm{Im}G_\ell(\omega) \tag{4.29a}$$

$$= \sum_{m,n=0}^{\infty} (p_m \pm p_n) \sum_{\alpha\in\mathbb{Z}} f_{m,n}^{(\alpha)} f_{m,n}^{(\alpha+\ell)*} \delta(\Delta\epsilon)\,. \tag{4.29b}$$

This equation yields the general spectral representation of Floquet response functions; it generalizes the Lehmann representation in equilibrium.

What can be deduced generally from (4.29)? For $\ell \neq 0$ we do not see any possibility for a general conclusion on positivity or reality of the spectral function. But for $\ell = 0$, it is obvious that

$$\rho_0(\omega) = \sum_{m,n=0}^{\infty} (p_m + p_n) \sum_{\alpha\in\mathbb{Z}} \left|f_{m,n}^{(\alpha)}\right|^2 \delta(\omega - \epsilon_n + \epsilon_m + \alpha\Omega) \geq 0 \tag{4.30a}$$

in the fermionic case, i.e., $\rho_0(\omega)$ is nonnegative and can hence be interpreted as density-of-states just like in equilibrium. This conclusion is closely related to Bochner's theorem [46]. Note that no general conclusion is possible in the bosonic case since the interplay of the factor $(p_m - p_n)$ and the shift $\alpha\Omega$ can be intricate. We stress that the case $\ell = 0$ corresponds precisely to the average of $\rho(\omega, t_{\mathrm{ave}})$ over one period of t_{ave} as we used previously in section 3.2 to reach physically meaningful results. Other authors have also averaged over one period to avoid negative spectral densities [23, 24], but without explaining why the results must be nonnegative. The above derivation puts this averaging procedure on a firm mathematical basis.

Sum rules are another useful spin-off from spectral representations. Using Eq. (4.29), we consider the zeroth-moment sum rule S and obtain

$$S \coloneqq \int_{-\infty}^{\infty} \rho_0(\omega) d\omega \tag{4.31a}$$

$$= \sum_{m,n=0}^{\infty} (p_m \pm p_n) \sum_{\alpha\in\mathbb{Z}} \left|f_{m,n}^{(\alpha)}\right|^2 \tag{4.31b}$$

$$= \frac{1}{T} \sum_{m,n=0}^{\infty} (p_m \pm p_n) \int_t^{t+T} |\Phi_{m,n}(t')|^2 dt' \tag{4.31c}$$

where the last step results from Parseval's identity. Re-inserting the definition from Eq. (4.18) for $\Phi_{m,n}(t)$ and using the completeness relation we derive in section 2.2 $\mathbb{1} = \sum_n |n,t\rangle \langle n,t|$, we arrive at the general sum rule

$$S = \frac{1}{T} \sum_m p_m \int_t^{t+T} \langle m,t'| \left[c, c^\dagger\right]_\pm |m,t'\rangle \, dt' \tag{4.32}$$

which is consistent with the value of $G(t+0,t)$ in (2.1) averaged over one period T. While in equilibrium, the sum rule is given by the expectation value of the (anti)commutator for (fermionic) bosonic operators, it is given by the temporal average in the Floquet regime. Hence, we find tangible evidence that the equivalent of a constant expectation value or a

constant spectral density at equilibrium is the temporal average of such an expectation value or of such a spectral function, respectively. The sum rules for higher moments of the spectral densities are commutators of products of operators in time so that they become convolutions after Fourier transformations in Floquet representation. Examples of such sum rules are given in Appendix B.

The sum rule in Eq. (4.32) is particularly meaningful if we consider fermionic or bosonic single-particle progagators, i.e., c is a single-particle annihilation operator and $c^\dagger$ the corresponding creation operator. Then, every expectation value on the right hand side equals unity and so does the temporal average and the weighted sum. Hence, the sum rule is indeed rigorously the same as in equilibrium for the averaged spectral functions. We then conclude that a fermionic spectral density in the Floquet regime can be interpreted to be a density-of-states similar to what happens in equilibrium. This has been used already in many numerical studies, see for instance Refs. [21, 22, 25].

Finally, we pass from the Wigner representation to the often employed equivalent Floquet representation. They are related by

$$G_{\ell j}(\omega) := G_{\ell - j}(\omega + (\ell + j)/2\Omega), \tag{4.33}$$

where $\ell, j \in \mathbb{Z}$ according to Tsuji et al. [25]. It is obvious that the Floquet representation does not contain more information than the Wigner representation. Indeed, the Floquet representation is redundant unless one restricts its argument ω to the interval $(-\Omega/2, \Omega/2]$ [25], but this restriction is not needed otherwise. Obviously, (4.33) implies that the physically meaningful averaged Green functions appearing in Wigner representation at index zero occur in Floquet representation on the diagonal, i.e., for $\ell = j$ one has $G_{\ell\ell}(\omega) = G_0(\omega + \ell\Omega)$ where different indices ℓ correspond to different shifts relative to G_{00}. This Green function and the spectral density $\rho_0(\omega)$ stemming from its imaginary part are generically studied in numerics [21, 22, 25] because they behave like equilibrium spectral densities. The negative spectral densities found in Ref. [25] for the gauge-invariant Green function may either be due to the gauge phase.

For completeness, we also provide the general expression for the non-diagonal Floquet representation of the retareded Green function. To obtain this expression, we first employ the shift $\ell \to \ell - j$ in Eq. (4.26c), yielding

$$\begin{aligned} G_{\ell-j}(\omega) = -i \sum_{m,n=0}^{\infty} (p_m \pm p_n) \sum_{\alpha} f^{(\alpha)}_{m,n} \left(f^{(\alpha+\ell-j)}_{m,n}\right)^* \times \\ \left\{ \pi\delta\left(\epsilon_m - \epsilon_n + \Omega\left(\alpha + \frac{\ell-j}{2}\right) + \omega\right) + i\mathrm{P}\left[\frac{1}{\epsilon_m - \epsilon_n + \Omega\left(\alpha + \frac{\ell-j}{2}\right) + \omega}\right] \right\}. \end{aligned} \tag{4.34}$$

Now we shift the frequency $\omega \to \omega + \Omega\left(\frac{\ell+j}{2}\right)$ and write the retarded Green function as a

Floquet matrix, as defined in Eq. (4.33)

$$G_{\ell j}(\omega) = G_{\ell - j}\left(\omega + \Omega\left(\frac{\ell + j}{2}\right)\right) \tag{4.35}$$

$$= -i \sum_{m,n=0}^{\infty} (p_m \pm p_n) \sum_{\alpha} f_{m,n}^{(\alpha)} \left(f_{m,n}^{(\alpha+\ell-j)}\right)^* \times \left\{\pi\delta(\epsilon_m - \epsilon_n + \omega + \Omega(\alpha+\ell)) + i\mathrm{P}\left[\frac{1}{\epsilon_m - \epsilon_n + \omega + \Omega(\alpha+\ell)}\right]\right\}, \tag{4.36}$$

or with $\alpha \to \alpha - \ell$

$$G_{\ell j}(\omega) = \sum_{m,n=0}^{\infty} (p_m \pm p_n) \sum_{\alpha} f_{m,n}^{(\alpha-\ell)} \left(f_{m,n}^{(\alpha-j)}\right)^* \times \left\{-i\pi\delta(\epsilon_m - \epsilon_n + \omega + \Omega\alpha) + \mathrm{P}\left[\frac{1}{\epsilon_m - \epsilon_n + \omega + \Omega\alpha}\right]\right\}. \tag{4.37}$$

The non-diagonal Floquet spectral functions $\rho_{\ell j}(\omega) = -(\pi)^{-1}\mathrm{Im}G_{\ell j}(\omega)$ are hence given by

$$\rho_{\ell j}(\omega) = \sum_{m,n=0}^{\infty} (p_m \pm p_n) \sum_{\alpha\in\mathbb{Z}} f_{m,n}^{(\alpha-\ell)} f_{m,n}^{(\alpha-j)*} (\omega - (\epsilon_n - \epsilon_m) + \alpha\Omega). \tag{4.38}$$

This expression helps to understand why one obtains a positive spectral function upon summing over all Floquet indices ℓ and j as done in Ref. [20]. Clearly

$$\rho_{\Sigma}(\omega) := \sum_{\ell,j\in\mathbb{Z}} \rho_{\ell j}(\omega) \tag{4.39a}$$

$$= \sum_{m,n=0}^{\infty} (p_m \pm p_n) \left|F_{m,n}\right|^2 \sum_{\alpha\in\mathbb{Z}} \delta(\omega - \epsilon_n + \epsilon_m + \alpha\Omega) \tag{4.39b}$$

which also yields a nonnegative spectral density with

$$F_{m,n} := \sum_{\ell\in\mathbb{Z}} f_{m,n}^{(\ell)} = \Phi_{m,n}(t=0). \tag{4.40}$$

Note that no dependence on α remains except a shift by $\alpha\Omega$. Thus, the sum over α on the right hand side of (4.39b) implies a divergence. But if we fix α to one single value or normalize with respect to the number of Floquet replica considered for this purpose, one obtains the neat sum rule

$$\sum_{m,n=0}^{\infty} (p_m \pm p_n) \left|F_{m,n}\right|^2 = \sum_{m} p_m \langle m,0| \left[c, c^\dagger\right]_{\pm} |m,0\} \tag{4.41a}$$

$$= \left\langle \left[c, c^\dagger\right]_{\pm} \right\rangle \Big|_{t=0} \tag{4.41b}$$

$$= 1 \tag{4.41c}$$

where the last equation holds for c a fermionic or bosonic single-particle annihilation operator only.

4.2 Dyson equation for periodically driven systems

The Dyson equation

$$G\left(t_1,t_2\right) \;=\; G^0\left(t_1,t_2\right)+\int \mathrm{d}t_3 \int \mathrm{d}t_4\, G^0\left(t_1,t_3\right)\Sigma\left(t_3,t_4\right)G\left(t_4,t_2\right) \tag{4.42}$$

connects the noninteracting Green function $G^0\left(t,t'\right)$ and the interacting Green function $G\left(t,t'\right)$ with the self energy $\Sigma\left(t,t'\right)$ [47]. The Green functions in Eq. (4.42) are retarded, but we suppress the Index R in order to simplify the notation. In equilibrium, a transformation from time space to energy space simplifies this equation significantly and allows one to solve for the interacting Green function in momentum space by a mere matrix inversion [48, 49]. Since we know about the properties of the imaginary part of the diagonal elements of the interacting Green function in the Floquet representation, it is useful to find the Floquet representation of the Dyson equation. The Wigner representation as given in Eq. (4.24) for the greater Green function can be generalized for any function $F(t,t')$ that satisfies $F(t,t')=F(t+T,t'+T)$. It is given by

$$F_n\left(\omega\right)=\frac{1}{T}\int_{-\infty}^{\infty}\mathrm{d}t_{\mathrm{rel}}\int_{-\frac{T}{2}}^{\frac{T}{2}}\mathrm{d}t_{\mathrm{ave}}e^{i\omega t_{\mathrm{rel}}}e^{i\frac{2\pi n}{T}t_{\mathrm{ave}}}F(t,t')\;, \tag{4.43}$$

so the reverse transformation yields

$$F(t,t')=\frac{1}{2\pi}\sum_n \exp\left[-i\frac{2\pi n}{T}\left(\frac{t+t'}{2}\right)\right]\int \mathrm{d}\omega \exp\left[-i\omega\left(t-t'\right)\right]F_n\left(\omega\right)\;. \tag{4.44}$$

We assume the self energy has the required periodicity and its Wigner representation $\Sigma_m\left(\omega\right)$ is connected to $\Sigma\left(t_3,t_4\right)$ by

$$\Sigma\left(t_3,t_4\right) \;=\; \frac{1}{2\pi}\sum_m \exp\left[-i\frac{2\pi m}{T}\left(\frac{t_3+t_4}{2}\right)\right]\left(\int \mathrm{d}\omega e^{-i\omega\left(t_3-t_4\right)}\Sigma_m\left(\omega\right)\right)\;. \tag{4.45}$$

In this case we can write the Dyson equation as

$$\begin{aligned} G\left(t_1,t_2\right) \;=\;& \frac{1}{2\pi}\sum_n \exp\left[-i\frac{2\pi n}{T}t_{\mathrm{ave}}\right]\left(\int \mathrm{d}\omega e^{-i\omega t_{\mathrm{rel}}}G_n^0\left(\omega\right)\right) \\ &+\frac{1}{2\pi}\sum_{n,m,l}\iiint \mathrm{d}\omega_a\mathrm{d}\omega_b\mathrm{d}\omega_c\, G_n^0\left(\omega_a\right)\Sigma_m\left(\omega_b\right)G_\ell\left(\omega_c\right) \\ &\exp\left[-it_{\mathrm{ave}}\left(\frac{n\pi}{T}+\omega_a+\frac{\ell\pi}{T}-\omega_c\right)\right]\exp\left[-\frac{it_{\mathrm{rel}}}{2}\left(\frac{n\pi}{T}+\omega_a-\frac{\ell\pi}{T}+\omega_c\right)\right] \\ &\delta\left(\frac{n\pi}{T}+\frac{m\pi}{T}-\omega_a+\omega_b\right)\delta\left(\frac{m\pi}{T}+\frac{\ell\pi}{T}-\omega_b+\omega_c\right)\;, \end{aligned} \tag{4.46}$$

where we used

$$\int_{-\infty}^{\infty}\mathrm{d}t_3\exp\left[-it_3\left(\frac{n\pi}{T}+\frac{m\pi}{T}-\omega_a+\omega_b\right)\right]=2\pi\delta\left(\frac{n\pi}{T}+\frac{m\pi}{T}-\omega_a+\omega_b\right) \tag{4.47}$$

and the analogous for the integration over t_4. The evaluation of the delta functions yields

$$\begin{aligned} 2\pi G\left(t_1,t_2\right) &= \sum_n \exp\left[-i\frac{2\pi n}{T}t_{\text{ave}}\right]\left(\int \mathrm{d}\omega e^{-i\omega t_{\text{rel}}} G_n^0\left(\omega\right)\right) \\ &+ \sum_{n,m,\ell}\int \mathrm{d}\omega\, G_n^0\left(\omega\right)\Sigma_m\left(\omega-\frac{n\pi}{T}-\frac{m\pi}{T}\right)G_\ell\left(\omega-\frac{\ell\pi}{T}-\frac{n\pi}{T}-\frac{2m\pi}{T}\right) \\ &\times\exp\left[-\frac{2\pi i t_{\text{ave}}}{T}\left(n+\ell+m\right)\right]\exp\left[-it_{\text{rel}}\left(\omega-\frac{\ell\pi}{T}-\frac{m\pi}{T}\right)\right] \end{aligned} \tag{4.48}$$

so we can calculate the reverse transformation given in Eq. (4.44) and obtain the Wigner representation of the Dyson Equation, which is given by

$$G_k\left(\tilde{\omega}\right) = \frac{1}{T}\int_{-\infty}^{\infty}\mathrm{d}t_{\text{rel}}\int_{-\frac{T}{2}}^{\frac{T}{2}}\mathrm{d}t_{\text{ave}}e^{i\tilde{\omega}t_{\text{rel}}}e^{i\frac{2\pi k}{T}t_{\text{ave}}} \tag{4.49a}$$

$$= G_k^0\left(\tilde{\omega}\right) \tag{4.49b}$$

$$+\sum_{n,m} G_n^0\left(\tilde{\omega}+\frac{k\pi}{T}-\frac{n\pi}{T}\right)\Sigma_m\left(\tilde{\omega}+\frac{k\pi}{T}-\frac{2n\pi}{T}-\frac{m\pi}{T}\right)G_{k-n-m}\left(\tilde{\omega}-\frac{n\pi}{T}-\frac{m\pi}{T}\right).$$

To get from the Wigner representation of the Dyson equation to the Floquet representation, we use the relation in Eq. (4.33) and the relation

$$G_{kn}\left(\omega\right) = G_{k-\ell,n-\ell}\left(\omega+\frac{2\pi\ell}{T}\right). \tag{4.50}$$

It requires several shifts in ω and the summation variables, namely (in this order) $n\to k-n$, $\omega\to\omega+\pi k/T$, $m\to n-m$, and the introduction of a new index ℓ via $k\to k-\ell$, $\omega\to\omega+2\pi\ell/T$, $m\to m-\ell$ and $n\to n-\ell$ to arrive at

$$G_{k\ell}\left(\omega\right) = G_{k\ell}^0\left(\omega\right)+\sum_{n,m}G_{k,n}^0\left(\omega\right)\Sigma_{n,m}\left(\omega\right)G_{m,l}\left(\omega\right). \tag{4.51}$$

This result is well known and can also be found in Ref. [25]. Now it is obvious that the Dyson equation can be written as a matrix equation

$$\underline{\underline{G}} = \underline{\underline{G}}^0+\underline{\underline{G}}^0\,\underline{\underline{\Sigma}}\,\underline{\underline{G}}, \tag{4.52}$$

where we are suppressing the ω dependence of the matrices to simplify the notation. Equation (4.52) is exactly analogous to the Dyson equation in equilibrium, and solving for the interacting Green function gives

$$\underline{\underline{G}} = \frac{1}{\left(\underline{\underline{G}}^0\right)^{-1}-\underline{\underline{\Sigma}}}. \tag{4.53}$$

The analogy between the Dyson equation in equilibrium and the nonequilibrium Dyson equation in Floquet representation illustrates that periodically driven systems share many formal properties with systems in equilibrium.

If we made the severe assumption that both $\underline{\underline{G}}^0$ and $\underline{\underline{\Sigma}}$ are diagonalizable and that $\underline{\underline{G}}^0$ has real eigenvalues (we will show this last property in the following for a specific model), the

sign of the imaginary part of $\underline{\underline{\Sigma}}$ would indeed determine the imaginary part of $\underline{\underline{G}}$, which would be another property that could be directly generalized from equilibrium to Floquet systems. Hence, knowing the sign of the imaginary part of $\underline{\underline{G}}$ would in turn allow to reach conclusions about the sign of the imaginary part of $\underline{\underline{\Sigma}}$.

Unfortunately, we are not aware of an argument that diagonalizability of $\underline{\underline{G}}^0$ and $\underline{\underline{\Sigma}}$ is generally given, therefore, next, we derive properties of the noninteracting, retarded Green function. In Ref. [25] it can be found that the inverse of the noninteracting Green function in Floquet matrix representation is given by

$$\left(G^{\mathrm{R}}\left(\boldsymbol{k}\right)\right)^{-1}_{mn}\left(\omega\right) = \begin{cases} \omega + n\Omega + \mu + i\eta - \varepsilon_0\left(\boldsymbol{k}\right) & \forall \quad n = m \\ -\varepsilon_{m-n}\left(\boldsymbol{k}\right) & \forall \quad n \neq m \end{cases}, \tag{4.54}$$

where the Wigner representation of the band structure $\varepsilon_{m-n}(\boldsymbol{k})$ in Eq. (3.5) is given by

$$\varepsilon_{m-n}(\boldsymbol{k}) = \int_{-\pi}^{\pi} \mathrm{d}z e^{i(m-n)z} \varepsilon\left(\boldsymbol{k} - e\boldsymbol{A}\left(\frac{z}{\Omega}\right)\right). \tag{4.55}$$

We specialize to a hypercubic lattice and a vector potential that lies along the diagonal, as we did in section 3.1, to use Eq. (3.11) and write the band structure as

$$\begin{aligned} \varepsilon_{m-n}(\boldsymbol{k}) =& \frac{1}{2\pi}\int_{-\pi}^{\pi} \mathrm{d}z \cos\left(\left(m-n\right)z\right)\left[\varepsilon(\boldsymbol{k})\cos\left(\frac{ea}{c}A\left(\frac{z}{\Omega}\right)\right) + \tilde{\varepsilon}(\boldsymbol{k})\sin\left(\frac{ea}{c}A\left(\frac{z}{\Omega}\right)\right)\right] \\ &+ \frac{i}{2\pi}\int_{-\pi}^{\pi} \mathrm{d}z \sin\left(\left(m-n\right)z\right)\left[\varepsilon(\boldsymbol{k})\cos\left(\frac{ea}{c}A\left(\frac{z}{\Omega}\right)\right) + \tilde{\varepsilon}(\boldsymbol{k})\sin\left(\frac{ea}{c}A\left(\frac{z}{\Omega}\right)\right)\right]. \end{aligned} \tag{4.56}$$

From the vector potential $\rho_\infty(t) = cE/\Omega\cos\left(\gamma t\right)$ as defined in (3.19), we can conclude that

$$A\left(\frac{z}{\Omega}\right) = \frac{cE}{\gamma}\cos(z) = \frac{cE_0}{ea\Omega}\cos(z), \tag{4.57}$$

which simplifies Eq. (4.56) because both $\cos\left[E_0/\Omega\cos(z)\right]$ and $\sin\left[E_0/\Omega\cos(z)\right]$ are even in z, while $\sin\left[\left(m-n\right)z\right]$ is odd in z. The integration in Eq. (4.56) runs over a symmetric interval in z, so the imaginary part vanishes and $\varepsilon_{m-n}(\boldsymbol{k})$ is a real function, given by

$$\varepsilon_{m-n}(\boldsymbol{k}) = \frac{1}{2\pi}\int_{-\pi}^{\pi} \mathrm{d}z \cos\left(\left(m-n\right)z\right)\left[\varepsilon(\boldsymbol{k})\cos\left(\frac{E_0}{\Omega}\cos(z)\right) + \tilde{\varepsilon}(\boldsymbol{k})\sin\left(\frac{E_0}{\Omega}\cos(z)\right)\right]. \tag{4.58}$$

At this point we define $E_\Omega = E_0/\Omega$ in order to simplify notation. Both integrations in Eq. (4.58) are related to the Bessel function of first kind by

$$\frac{1}{2\pi}\int_{-\pi}^{\pi} \mathrm{d}z \cos\left(az\right)\cos\left(E_\Omega\cos(z)\right) = \begin{cases} 0 & \forall a = \text{odd} \\ -J_{|a|}\left(E_\Omega\right) & \forall a = \text{even}, a \bmod 4 = 2 \\ J_{|a|}\left(E_\Omega\right) & \forall a = \text{even}, a \bmod 4 = 0 \end{cases} \tag{4.59}$$

$$\frac{1}{2\pi}\int_{-\pi}^{\pi} \mathrm{d}z \cos\left(az\right)\sin\left(E_\Omega\cos(z)\right) = \begin{cases} 0 & \forall a = \text{even} \\ J_{|a|}\left(E_\Omega\right) & \forall a = \text{odd}, (a+1) \bmod 4 = 2 \\ -J_{|a|}\left(E_\Omega\right) & \forall a = \text{odd}, (a+1) \bmod 4 = 0 \end{cases}. \tag{4.60}$$

The Floquet matrix representation $\varepsilon_{mn}(\boldsymbol{k}) = \varepsilon_{m-n}(\boldsymbol{k})$ of the band structure is hence given by

$$\varepsilon_{mn}(\boldsymbol{k}) = \begin{bmatrix} \ddots & \vdots & \vdots & \vdots & \vdots & \iddots \\ \dots & +\varepsilon(\boldsymbol{k})J_0(E_\Omega) & +\tilde{\varepsilon}(\boldsymbol{k})J_1(E_\Omega) & -\varepsilon(\boldsymbol{k})J_2(E_\Omega) & -\tilde{\varepsilon}(\boldsymbol{k})J_3(E_\Omega) & \dots \\ \dots & +\tilde{\varepsilon}(\boldsymbol{k})J_1(E_\Omega) & +\varepsilon(\boldsymbol{k})J_0(E_\Omega) & +\tilde{\varepsilon}(\boldsymbol{k})J_1(E_\Omega) & -\varepsilon(\boldsymbol{k})J_2(E_\Omega) & \dots \\ \dots & -\varepsilon(\boldsymbol{k})J_2(E_\Omega) & +\tilde{\varepsilon}(\boldsymbol{k})J_1(E_\Omega) & +\varepsilon(\boldsymbol{k})J_0(E_\Omega) & +\tilde{\varepsilon}(\boldsymbol{k})J_1(E_\Omega) & \dots \\ \dots & -\tilde{\varepsilon}(\boldsymbol{k})J_3(E_\Omega) & -\varepsilon(\boldsymbol{k})J_2(E_\Omega) & +\tilde{\varepsilon}(\boldsymbol{k})J_1(E_\Omega) & +\varepsilon(\boldsymbol{k})J_0(E_\Omega) & \dots \\ \iddots & \vdots & \vdots & \vdots & \vdots & \ddots \end{bmatrix}, \tag{4.61}$$

which differs from the result presented in Ref. [25] only by a unitary matrix transformation $\underline{\underline{\varepsilon}} = \underline{\underline{M}}^{-1}\,\underline{\underline{\tilde{\varepsilon}}}\,\underline{\underline{M}}$ with the transformation matrix

$$\underline{\underline{M}} = \begin{bmatrix} \ddots & \vdots & \vdots & \vdots & \vdots & \iddots \\ \dots & 1 & 0 & 0 & 0 & \dots \\ \dots & 0 & i & 0 & 0 & \dots \\ \dots & 0 & 0 & -1 & 0 & \dots \\ \dots & 0 & 0 & 0 & -i & \dots \\ \iddots & \vdots & \vdots & \vdots & \vdots & \ddots \end{bmatrix}. \tag{4.62}$$

This means that the Floquet matrix representation of the inverse noninteracting Green function as defined in Eq. (4.54) has merely an infinitesimal imaginary part for a hypercubic lattice and a sinusoidal driving. This statement can be extended to the noninteracting Green function since the inverse of a real matrix is real. The Dyson equation (4.52) can therefore be separated into a real and an imaginary part, where

$$\operatorname{Im}\left[\underline{\underline{G}}\right] = \underline{\underline{G}}^0\left(\operatorname{Re}\left[\underline{\underline{\Sigma}}\right]\operatorname{Im}\left[\underline{\underline{G}}\right] + \operatorname{Im}\left[\underline{\underline{\Sigma}}\right]\operatorname{Re}\left[\underline{\underline{G}}\right]\right). \tag{4.63}$$

Since we know that the diagonal elements of the Green function in Floquet matrix representation have an imaginary part that is smaller or equal to zero, we can conclude that

$$\operatorname{Tr}\left[\underline{\underline{G}}^0\left(\operatorname{Re}\left[\underline{\underline{\Sigma}}\right]\operatorname{Im}\left[\underline{\underline{G}}\right] + \operatorname{Im}\left[\underline{\underline{\Sigma}}\right]\operatorname{Re}\left[\underline{\underline{G}}\right]\right)\right] \leq 0\,. \tag{4.64}$$

One can also start from the Dyson equation that is solved for the Green function, as given in Eq. (4.53), where it is useful to recall the identity

$$\frac{1}{\underline{A} \pm i\underline{B}} = \frac{1}{\underline{A} + \underline{B}\,\underline{A}^{-1}\,\underline{B}}\left(\mathbb{1} \mp i\underline{\underline{A}}^{-1}\underline{\underline{B}}\right) \qquad \forall \underline{\underline{A}}, \underline{\underline{B}} \in \underline{\underline{\mathbb{R}}}\,. \tag{4.65}$$

This allows to calculate the imaginary part of the Green function and conclude that

$$\operatorname{Tr}\left[\frac{\left[\left(\underline{\underline{G}}^0\right)^{-1} - \operatorname{Re}\left(\underline{\underline{\Sigma}}\right)\right]^{-1}\operatorname{Im}\left(\underline{\underline{\Sigma}}\right)}{\left(\underline{\underline{G}}^0\right)^{-1} - \operatorname{Re}\left(\underline{\underline{\Sigma}}\right) + \operatorname{Im}\left(\underline{\underline{\Sigma}}\right)\left[\left(\underline{\underline{G}}^0\right)^{-1} - \operatorname{Re}\left(\underline{\underline{\Sigma}}\right)\right]^{-1}\operatorname{Im}\left(\underline{\underline{\Sigma}}\right)}\right] \leq 0\,. \tag{4.66}$$

Note that Eq. (4.66) requires $\left[\left(\underline{\underline{G}}^0\right)^{-1} - \operatorname{Re}\left(\underline{\underline{\Sigma}}\right)\right]$ to be invertible. But even though these statements about the trace can be deduced mathematically, there is no obvious analogy to equilibrium, where the sign of the imaginary part of the Green function can be directly deduced from the sign of the imaginary part of the interacting Green function. As stated above, such a connection only exists if both $\underline{\underline{G}}^0$ and $\underline{\underline{\Sigma}}$ are diagonalizable.

5 Summary and outlook

In this thesis, we have examined situations where one might be able to observe Floquet behavior for both interacting and noninteracting systems. We studied noninteracting, fermionic systems (which do not heat up) in chapter 3 and compared the exact Floquet solutions for the retarded Green functions to a number of different cases including a semi-infinite drive and a periodic drive with a Gaussian envelope (to make it into a pulse which is experimentally realizable). The true Floquet system has a Hamiltonian that is periodic with respect to the period of the driving.

We observed a number of interesting results. First, for the pure Floquet system, the conventional definition of the instantaneous DOS as the imaginary part of the retarded local Green function evaluated at fixed t_{ave} or t_2, is not positive semi-definite. But the time-averaged density of states always is. This holds both for the diagonal and the horizontal Green function.

Second, when an ac electric field is applied along the main diagonal direction of the lattice, the value of the Bessel function $J_0\left(E_0/\gamma\right)$ is critical in determining the subsequent behavior. In the Floquet limit, one will obtain a local DOS that is a sequence of delta functions when $J_0\left(E_0/\gamma\right) = 0$; they become broadened and lose their identity as J_0 becomes larger in magnitude.

Third, even if the Hamiltonian is not strictly periodic, Floquet theory is still applicable as a good approximation if certain other requirements are met. In particular, when $\left|J_0\left(E_0/\gamma\right)\right|$ is large, the pulsed system appears quite close to the Floquet result. But, as mentioned above, when we are at a zero of the Bessel function, it is never feasible to find the pumped system looking like the Floquet one.

In particular, if we employ a Gaussian envelope function, the width of the envelope is the primary predictor of whether the system will look like a periodic Floquet system. A wide Gaussian ensures that the measured DOS resembles the DOS of the infinitely driven system, even if the frequency of the driving field is low. On the other hand, measuring at high frequencies does not compensate for a narrow Gaussian. Hence, it is not true that one can simply count the number of oscillations inside one or two standard deviations of the pulse to determine whether it will behave like a Floquet system—this only holds if the Gaussian pulse width is wide enough.

Surprisingly, even if the system resembles a periodic Floquet system in the time domain, it is not sufficient to average the DOS over one period of the driving (in t_{ave} or t_2) to reproduce the DOS of the corresponding Floquet Hamiltonian (even if the amplitude E_0, the frequency γ and the width of the Gaussian t_E are optimally chosen). Instead, it further requires a second averaging, precisely the running average (in the frequency domain) over one period of the oscillations, for the pulsed DOS to resemble the DOS of the infinite drive.

As interactions are added in (see as a first step Ref. [14]), we expect it to be easier for the Gaussian pumped system to look Floquet like, because the extra scattering due to the interactions will cause the Green functions to decay more rapidly in relative time. This will, in turn, widen the parameter space where the pulsed system appears to behave more like the corresponding Floquet system. If the pump adds substantial heat to the system a high temperature stationary state will be reached in which we do not expect the retarded Green function to depend strongly on temperature. Of course it will have larger effect on lesser Green functions, but we are not discussing those here. We look forward to seeing more experiments that will illustrate this behavior in the future.

In chapter 4, we considered a broad range of nonequilibrium systems (including interacting systems) which are in the Floquet regime, i.e., they are given in a mixture of quasi-stationary Floquet states which solve the time-dependent Schrödinger equation. For this setting, we rigorously established a generalization of the Lehmann representation. The spectral representation of two-time Floquet response functions include the cases of fermionic and bosonic single-particle propagators. We clarified the relation to the Wigner representation, which exploits the periodicity in the average time of the two times and to the Floquet representation.

Our results in section 4.1 show precisely when fermionic spectral functions must be nonnegative and can be interpreted as densities-of-states. We also established some exact sum rules.

When studying the Dyson equation for periodically driven systems in section 4.2, we found an analogy between the Dyson equation in equilibrium and the nonequilibrium Dyson equation in Floquet representation, which illustrates that periodically driven systems share many formal properties with systems in equilibrium. But despite the fact that in equilibrium one deduces from the Dyson equation that the imaginary part of the self-energy is nonnegative, no similar result holds in the Floquet regime. Conclusions about the imaginary part of the nonequilibrium self energy are not possible, unless certain assumptions about the diagonalizability of the self energy and the noninteracting Green function are made.

As an outlook, we think that more information on the mathematical properties of the self-energy in the Floquet regime is also desirable. One might conjecture that the self-energy averaged over t_{ave} should also behave as in equilibrium. But the Floquet Dyson equation is too complicated and does not appear to permit one to establish this fact.

A Convolution of periodic functions

We start with two arbitrary $2\pi/\gamma$ periodic functions $f(t)$ and $g(t)$, which can be expressed as the following Fourier series:

$$f(t) = \sum_m e^{im\gamma t} f_m \tag{A.1a}$$

$$g(t) = \sum_m e^{im\gamma t} g_m \,. \tag{A.1b}$$

The convolution of these two functions is given by

$$h(t) = \frac{\gamma}{2\pi} \int_x^{x+\frac{2\pi}{\gamma}} g(t-t')\, f(t')\, \mathrm{d}t' \tag{A.2a}$$

$$= \frac{\gamma}{2\pi} \int_x^{x+\frac{2\pi}{\gamma}} \sum_{m,n} e^{in\gamma(t-t')} e^{im\gamma t'} g_n f_m \mathrm{d}t' \tag{A.2b}$$

$$= \sum_{m,n} g_n f_m e^{int\gamma} \underbrace{\frac{\gamma}{2\pi} \int_x^{x+\frac{2\pi}{\gamma}} e^{i\gamma(m-n)t'} \mathrm{d}t'}_{\delta_{m,n}} \tag{A.2c}$$

$$= \sum_m g_m f_m e^{imt\gamma} \tag{A.2d}$$

$$= \sum_m h_m e^{imt\gamma} \,. \tag{A.2e}$$

which is also $2\pi/\gamma$ periodic and has Fourier coefficients $h_m = g_m f_m$. This means that if the coefficients f_m and g_m are complex conjugates of each other, the coefficients of the convolution are positive and obey $h_m = |f_m|^2 \geq 0$. Coefficients that are complex conjugates naturally arise when the $2\pi/\gamma$ periodic functions obey $g(t) = f^*(-t) = \sum_m \exp[im\gamma t] f_m^*$. Using this identity and substituting either $\tilde{t} = t' - t$ or $\tilde{\tilde{t}} = t' - (t/2)$, the convolution becomes

$$h(t) = \frac{\gamma}{2\pi} \int_x^{x+\frac{2\pi}{\gamma}} f^*(t'-t)\, f(t')\, \mathrm{d}t' \tag{A.3a}$$

$$= \frac{\gamma}{2\pi} \int_{\tilde{x}}^{\tilde{x}+\frac{2\pi}{\gamma}} f^*\left(\tilde{t}\right) f\left(\tilde{t}+t\right) \mathrm{d}\tilde{t} \tag{A.3b}$$

$$= \frac{\gamma}{2\pi} \int_{\tilde{\tilde{x}}}^{\tilde{\tilde{x}}+\frac{2\pi}{\gamma}} f^*\left(\tilde{\tilde{t}} - \frac{t}{2}\right) f\left(\tilde{\tilde{t}} + \frac{t}{2}\right) \mathrm{d}\tilde{\tilde{t}} \tag{A.3c}$$

$$= \sum_m |f_m|^2 e^{imt\gamma} \,. \tag{A.3d}$$

The averaged local retarded Green's function, as defined in Eq. (3.30) of the infinitely driven field, has exactly the form of Eq. (A.3b) when the retarded Green's function is given as a function of t_1 and t_2 by identifying $t_2 = \tilde{t}$. At the same time it has exactly the form of (A.3c) when writing the retarded Green's function as a function of t_{ave} and t_{rel} and identifying $t_{\mathrm{ave}} = \tilde{\tilde{t}}$. Therefore the time-averaged local retarded Green's function is given by

$$\bar{G}^R(\boldsymbol{k}, t_{\mathrm{rel}}) = -\frac{i}{\hbar}\Theta(t_{\mathrm{rel}})\, e^{-\frac{i\varepsilon(\boldsymbol{k})}{\hbar} J_0\left(\frac{E_0}{\hbar}\right) t_{\mathrm{rel}}} \sum_m |f_m|^2\, e^{imt_{\mathrm{rel}}\gamma} \tag{A.4a}$$

no matter which Fourier transform is chosen. The averaged spectral function as defined in Eq. (3.31a) yields

$$\bar{\rho}(\omega, \boldsymbol{k}) = -\frac{1}{\pi}\mathrm{Im}\left[-\frac{i}{\hbar}\sum_m |f_m|^2 \lim_{\eta\to 0^+} \int_0^\infty e^{it_{\mathrm{rel}}\left(\omega + m\gamma - \frac{\varepsilon(\boldsymbol{k})}{\hbar} J_0\left(\frac{E_0}{\hbar}\right) + i\eta\right)} \mathrm{d}\, t_{\mathrm{rel}}\right] \tag{A.5a}$$

$$= \sum_m \frac{|f_m|^2}{\hbar} \delta\left(\omega + m\gamma - \frac{\varepsilon(\boldsymbol{k})}{\hbar} J_0\left(\frac{E_0}{\hbar}\right)\right). \tag{A.5b}$$

This is manifestly nonnegative and completes the proof.

B Sum rules for higher moments of the spectral densities in the Hubbard model

We already discussed the zeroth moment sum rule in Eq. (19), which is valid for any given Hamiltonian. To analyze higher spectral moment sum rules, we have to specify the underlying model, as the sum rules depend on the particular form of the Hamiltonian. Here we will present results for the Hubbard Hamiltonian, which is one of the simplest models to describe electron-electron interactions. Furthermore, it is a model for which the sum rules are well-known [50]. The Hubbard-Hamiltonian is given by

$$\mathcal{H}_{\mathrm{H}}(t) = -\sum_{ij\sigma} t_{ij}(t)\, c^{\dagger}_{i\sigma} c_{j\sigma} + \sum_{i} U_i(t)\, n_{i\downarrow} n_{i\uparrow} - \sum_{i} \mu_i(t) \left(n_{i\downarrow} + n_{i\uparrow}\right) \tag{B.1}$$

where $t_{ij}(t)$ is the time-dependent Hermitian electron hopping matrix, $U_i(t)$ is the time-dependent on-site Hubbard repulsion, and $\mu_i(t)$ is a time-dependent local site energy. To simplify the formulas, we introduce the notation $\left[\tilde{O} = \hat{O}(t_{\mathrm{ave}})\right]$ to indicate the operator (or function) is evaluated at the average time t_{ave} after taking the limit $t_{\mathrm{rel}} \to 0$. We assume that $\tilde{t}_{ij}$, $\tilde{U}_i$ and $\tilde{\mu}_i$ are T periodic in t_{ave} and therefore can be written as a Fourier series

$$\tilde{t}_{ij} = \sum_{n} t^{n}_{ij} \exp\left[in\frac{2\pi}{T}t\right] \tag{B.2}$$

(analogous for $\tilde{U}_i$ and $\tilde{\mu}_i$). The zeroth moment sum rule is given by $\mu^{R0}_{ij\sigma}(t_{\mathrm{ave}}) = \delta_{ij}$, so integrating over one period

$$\frac{1}{T}\int_{x}^{x+T} \mu^{R0}_{ij\sigma}(t_{\mathrm{ave}})\, \mathrm{d}t_{\mathrm{ave}} = \delta_{ij} \tag{B.3}$$

does not change the result. This is different for the first moment, which is given by

$$\mu^{R1}_{ij\sigma}(t_{\mathrm{ave}}) = -\tilde{t}_{ij} - \delta_{ij}\tilde{\mu}_i + \delta_{ij}\tilde{U}_i \left\langle \tilde{n}_{i\bar{\sigma}} \right\rangle , \tag{B.4}$$

so the integration yields

$$\frac{1}{T}\int_{t}^{t+T} \mu^{R1}_{ij\sigma}(t_{\mathrm{ave}})\, \mathrm{d}t_{\mathrm{ave}} = t^{0}_{ij} - \delta_{ij}\mu^{0}_{i}\delta_{ij} \sum_{m} U^{m}_{i} \left\langle n_{i\bar{\sigma}} \right\rangle^{-m} .$$

The second moment sum rule is given by

$$\begin{aligned} \mu^{R2}_{ij\sigma}(t_{\mathrm{ave}}) \;=\; & \sum_{k} \tilde{t}_{ik}\tilde{t}_{kj} + \tilde{t}_{ij}\tilde{\mu}_i + \tilde{t}_{ij}\tilde{\mu}_j - \tilde{t}_{ij}\tilde{U}_i \left\langle \tilde{n}_{i\bar{\sigma}} \right\rangle - \tilde{t}_{ij}\tilde{U}_j \left\langle \tilde{n}_{j\bar{\sigma}} \right\rangle \\ & + \delta_{ij}\left(\tilde{\mu}_i^2 + \tilde{U}_i^2 \left\langle \tilde{n}_{i\bar{\sigma}} \right\rangle^2 - 2\tilde{\mu}_i\tilde{U}_i \left\langle \tilde{n}_{i\bar{\sigma}} \right\rangle\right) + \delta_{ij}\left(\tilde{U}_i^2 \left\langle \tilde{n}_{i\bar{\sigma}} \right\rangle - \tilde{U}_i^2 \left\langle \tilde{n}_{i\bar{\sigma}} \right\rangle^2\right) \end{aligned} \tag{B.5}$$

which, when integrated over one period becomes

$$\begin{aligned}\frac{1}{T}\int_x^{x+T}\mu^{R2}_{ij\sigma}\left(t_{\text{ave}}\right)\,\mathrm{d}t_{\text{ave}} &= \sum_{k,n} t^n_{ik}t^{-n}_{kj}+\sum_n\left(t^n_{ij}\mu^{-n}_i+t^n_{ij}\mu^{-n}_j\right) \\ &-\sum_{nm}\left(t^{n+m}_{ij}U^{-n}_i\left\langle n_{i\bar{\sigma}}\right\rangle^{-m}+t^{n+m}_{ij}U^{-n}_j\left\langle n_{j\bar{\sigma}}\right\rangle^{-m}\right)+\delta_{ij}\sum_n\left|\mu^n_i\right|^2 \\ &-2\delta_{ij}\sum_{mn}\mu^{n+m}_i U^{-n}_i\left\langle n_{i\bar{\sigma}}\right\rangle^{-m}+\delta_{ij}\sum_{mn}U^{n+m}_i U^{-n}_i\left\langle n_{i\bar{\sigma}}\right\rangle^{-m}\,.\end{aligned} \tag{B.6}$$

It is obvious that the mixing of Floquet coefficients increases as we go to higher moments. Finally we would like to discuss the zeroth moment of the self energy, given by

$$C^{R0}_{ij\sigma}\left(t_{\text{ave}}\right) = \delta_{ij}\left(\tilde{U}^2_i\left\langle\tilde{n}_{i\bar{\sigma}}\right\rangle-\tilde{U}^2_i\left\langle\tilde{n}_{i\bar{\sigma}}\right\rangle^2\right)\,. \tag{B.7}$$

Here the integration over one period yields

$$\frac{1}{T}\int_x^{x+T}C^{R0}_{ij\sigma}\left(t_{\text{ave}}\right)\,\mathrm{d}t_{\text{ave}}=\delta_{ij}\sum_{mn}U^{n+m}_i U^{-n}_i\left\langle n_{i\bar{\sigma}}\right\rangle^{-m}-\delta_{ij}\sum_{lmn}U^{l+m+n}_i U^{-l}_i\left\langle n_{i\bar{\sigma}}\right\rangle^{-m}\left\langle n_{i\bar{\sigma}}\right\rangle^{-l},$$

so even for the lowest moment of the self energy, the Fourier coefficients of $\tilde{U}_i$ and $\tilde{n}_i$ mix.

Bibliography

[1] I. Bloch, J. Dalibard, and W. Zwerger, "Many-body physics with ultracold gases", Rev. Mod. Phys. **80**, 885 (2008).

[2] T. Esslinger, "Fermi-Hubbard Physics with Atoms in an Optical Lattice", Annual Review of Condensed Matter Physics **1**, 129 (2010).

[3] V. Axt and T. Kuhn, "Femtosecond spectroscopy in semiconductors: a key to coherences, correlations and quantum kinetics", Reports on Progress in Physics **67**, 433 (2004).

[4] L. Perfetti, P. A. Loukakos, M. Lisowski, U. Bovensiepen, H. Berger, S. Biermann, P. S. Cornaglia, A. Georges, and M. Wolf, "Time Evolution of the Electronic Structure of 1T -TaS_2 through the Insulator-Metal Transition", Phys. Rev. Lett. **97**, 067402 (2006).

[5] A. Kirilyuk, A. V. Kimel, and T. Rasing, "Ultrafast optical manipulation of magnetic order", Rev. Mod. Phys. **82**, 2731 (2010).

[6] G. Floquet, "Sur les équations différentielles linéaires à coefficients périodiques", fre, Annales scientifiques de l'École Normale Supérieure **12**, 47 (1883).

[7] M. Grifoni and P. Hänggi, "Driven quantum tunneling", Physics Reports **304**, 229 (1998).

[8] P. Hänggi, "Driven Quantum Systems", in Quantum transport and dissipation, edited by T. Dittrich, P. Hänggi, G.-L. Ingold, B. Kramer, G. Schön, and W. Zwerger (1998).

[9] N. H. Lindner, G. Refael, and V. Galitski, "Floquet topological insulator in semiconductor quantum wells", Nature Physics **7**, 490 (2011).

[10] T. Kitagawa, E. Berg, M. Rudner, and E. Demler, "Topological characterization of periodically driven quantum systems", Phys. Rev. B **82**, 235114 (2010).

[11] M. A. Sentef, M. Claassen, A. F. Kemper, B. Moritz, T. Oka, J. K. Freericks, and T. P. Devereaux, "Theory of Floquet band formation and local pseudospin textures in pump-probe photoemission of graphene", Nature Communications **6**, 7047 (2015).

[12] J. Mentink, K. Balzer, and M. Eckstein, "Ultrafast and reversible control of the exchange interaction in Mott insulators", Nature communications **6**, 6708 (2015).

[13] M. Puviani and F. Manghi, "Periodically driven interacting electrons in one dimension: Many-body Floquet approach", Phys. Rev. B **94**, 161111 (2016).

[14] D. M. Kennes, A. de la Torre, A. Ron, D. Hsieh, and A. J. Millis, "Floquet Engineering in Quantum Chains", Phys. Rev. Lett. **120**, 127601 (2018).

[15] Y. H. Wang, H. Steinberg, P. Jarillo-Herrero, and N. Gedik, "Observation of Floquet-Bloch states on the surface of a topological insulator", Science **342**, 453 (2013).

[16] B. M. Fregoso, Y. H. Wang, N. Gedik, and V. Galitski, "Driven electronic states at the surface of a topological insulator", Phys. Rev. B **88**, 155129 (2013).

[17] M. Claassen, C. Jia, B. Moritz, and T. P. Devereaux, "All-optical materials design of chiral edge modes in transition-metal dichalcogenides", Nature Communications **7**, Article, 13074 EP (2016).

[18] S. Tang, C. Zhang, D. Wong, Z. Pedramrazi, H.-Z. Tsai, C. Jia, B. Moritz, M. Claassen, H. Ryu, S. Kahn, J. Jiang, H. Yan, M. Hashimoto, D. Lu, R. G. Moore, C.-C. Hwang, C. Hwang, Z. Hussain, Y. Chen, M. M. Ugeda, Z. Liu, X. Xie, T. P. Devereaux, M. F. Crommie, S.-K. Mo, and Z.-X. Shen, "Quantum spin Hall state in monolayer 1T′ -WTe_2", Nature Physics **13**, 683 (2017).

[19] Y. H. Wang, H. Steinberg, P. Jarillo-Herrero, and N. Gedik, "Observation of Floquet-Bloch States on the Surface of a Topological Insulator", Science **342**, 453 (2013).

[20] R. Frank, "Quantum criticality and population trapping of fermions by non-equilibrium lattice modulations", New Journal of Physics **15**, 123030 (2013).

[21] T. Qin and W. Hofstetter, "Spectral functions of a time-periodically driven Falicov-kimball model: Real-space Floquet dynamical mean-field theory study", Phys. Rev. B **96**, 075134 (2017).

[22] T. Qin and W. Hofstetter, "Nonequilibrium steady states and resonant tunneling in time-periodically driven systems with interactions", Phys. Rev. B **97**, 125115 (2018).

[23] K. Pototzky and E. Gross, "How to interpret the spectral density of the Keldysh nonequilibrium Green's function", arXiv preprint arXiv:1405.5984 (2014).

[24] M. Genske, "Periodically driven many-body quantum systems: Quantum ratchets, Topological States and the Floquet-Boltzmann Equation", PhD thesis, Universität zu Köln (2017).

[25] N. Tsuji, T. Oka, and H. Aoki, "Correlated electron systems periodically driven out of equilibrium: Floquet + DMFT formalism", Phys. Rev. B **78**, 235124 (2008).

[26] R. Peierls, "Zur Theorie des Diamagnetismus von Leitungselektronen", Zeitschrift für Physik **80**, 763 (1933).

[27] H. Aoki, N. Tsuji, M. Eckstein, M. Kollar, T. Oka, and P. Werner, "Nonequilibrium dynamical mean-field theory and its applications", Rev. Mod. Phys. **86**, 779 (2014).

[28] J. K. Freericks, V. M. Turkowski, and V. Zlatić, "Nonequilibrium Dynamical Mean-Field Theory", Phys. Rev. Lett. **97**, 266408 (2006).

[29] G. Stefanucci and R. van Leeuwen, *Nonequilibrium Many-body Theory of Quantum Systems: A Modern Introduction* (Cambridge University Press, Cambridge, UK, 2013).

[30] K. Najafi, "Nonlinear Response of Strongly Interacting Quantum Systems in Nonequilibrium", PhD thesis, Georgetown University (2018).

[31] R. Kubo, M. Toda, and N. Hashitsume, *Statistical physics ii: nonequilibrium statistical mechanics*, Vol. 31 (Springer Science & Business Media, 2012).

[32] A. V. Joura, "Static and dynamic properties of strongly correlated lattice models under electric fields (Dynamical Mean Field Theory approach)", PhD thesis, Georgetown University (2014).

[33] V. Turkowski and J. K. Freericks, "Nonlinear response of Bloch electrons in infinite dimensions", Phys. Rev. B **71**, 085104 (2005).

[34] J. K. Freericks and H. R. Krishnamurthy, "Constant Matrix Element Approximation to Time-Resolved Angle-Resolved Photoemission Spectroscopy", Photonics **3**, 58 (2016).

[35] J. K. Freericks, H. R. Krishnamurthy, and T. Pruschke, "Theoretical Description of Time-Resolved Photoemission Spectroscopy: Application to Pump-Probe Experiments", Phys. Rev. Lett. **102**, 136401 (2009).

[36] C. Gruber, N. Macris, P. Royer, and J. K. Freericks, "Higher period ordered phases on the Bethe lattice", Phys. Rev. B **63**, 165111 (2001).

[37] E. Wigner, "On the Quantum Correction for Thermodynamic Equilibrium", Phys. Rev. **40**, 749 (1932).

[38] J. H. Shirley, "Solution of the Schrödinger Equation with a Hamiltonian Periodic in Time", Phys. Rev. **138**, B979 (1965).

[39] M. Beck, H. Schäfer, G. Klatt, J. Demsar, S. Winnerl, M. Helm, and T. Dekorsy, "Impulsive terahertz radiation with high electric fields from an amplifier-driven large-area photoconductive antenna", Opt. Express **18**, 9251 (2010).

[40] J. Debus, private communication, 2018.

[41] J. C. Slater and G. F. Koster, "Simplified LCAO Method for the Periodic Potential Problem", Phys. Rev. **94**, 1498 (1954).

[42] W. Metzner and D. Vollhardt, "Correlated Lattice Fermions in $d = \infty$ Dimensions", Phys. Rev. Lett. **62**, 324 (1989).

[43] J. D. Jackson and L. B. Okun, "Historical roots of gauge invariance", Rev. Mod. Phys. **73**, 663 (2001).

[44] A. P. Jauho and J. W. Wilkins, "Theory of high-electric-field quantum transport for electron-resonant impurity systems", Phys. Rev. B **29**, 1919 (1984).

[45] G. Czycholl, *Theoretische Festkörperphysik Band 1*, 4th ed. (Springer Spektrum, 2016).

[46] S. Bochner, ed., *Fouriersche Integrale* (Akademische Verlagsgesellschaft m b. H., Leipzig, Germany, 1932).

[47] L. V. Keldysh et al., "Diagram technique for nonequilibrium processes", Sov. Phys. JETP **20**, 1018 (1965).

[48] G. Rickayzen, *Green's Functions and Condensed Matter* (Academic Press Limited, London, United Kingdom, 1980).

[49] P. Coleman, *Introduction to Many-Body Physics* (Cambridge University Press, 2015).

[50] V. Turkowski and J. K. Freericks, "Nonequilibrium sum rules for the retarded self-energy of strongly correlated electrons", Phys. Rev. B **77**, 205102 (2008).

Acknowledgements

I would like to express my gratitude to numerous colleagues and friends, who helped me in the course of my master studies. Their helpful thoughts and valuable insights certainly influenced this thesis to a large extent.

Above all, I'd like to thank my supervisors Götz Uhrig and Jim Freericks for their support and their guidance when writing this thesis, and for introducing me to the fascinating topic of nonequilibrium physics. Throughout the last year, I have learned enormously from them, and it was a huge honor that they gave me the chance to study with them, both at TU Dortmund and at Georgetown University. In this context, I'd also like to express my gratitude towards the Studienstiftung des deutschen Volkes, whose financial support not only allowed me to completely concentrate on my work, but also made my stay in Washington D.C. possible.

In Dortmund, I'd like to thank my colleges Mohsen Yarmohammadi and Philipp Schering. I consider myself lucky to have shared an office with them, and my work benefited greatly from our numerous discussions on the whiteboard, as they often helped me to approach problems from a different angle and opened my eyes to possible complications. Furthermore Philipp Schering put a lot of time and large efforts into any technical problems that I encountered during this thesis.

My time at Georgetown University would not have been the same without the help of Khadijeh Sona Najafi, who patiently answered all my questions about nonequilibrium Green functions and soon became my very first friend in Washington. I'm also grateful to Daniel O'Brian for introducing me to the graduate students at the Department of Physics. I think I can safely say that the friendly and encouraging atmosphere in our office helped all of us to work productively.

Outside of University I owe great thanks to Alex Lestsantear, who did not only accompany me on many hikes through numerous National Parks, but who also proofread this master thesis. Our valuable discussions and shared adventures certainly helped to sort my thoughts and feel at home in Washington. In Wuppertal I'd like to thank Leona Flohr, who has always been a great friend to me, and who encouraged me whenever I was frustrated or downhearted.

Last but not least, I would like to thank my parents Petra and Rolf for their endless support and their encouragement to pursue my dreams. Dear Mum, none of this would exist without you!

Eidesstattliche Versicherung

Ich versichere hiermit an Eides statt, dass ich die vorliegende Abschlussarbeit mit dem Titel "Floquet behavior for lattice fermions driven by light" selbstständig und ohne unzulässige fremde Hilfe erbracht habe. Ich habe keine anderen als die angegebenen Quellen und Hilfsmittel benutzt, sowie wörtliche und sinngemäße Zitate kenntlich gemacht. Die Arbeit hat in gleicher oder ähnlicher Form noch keiner Prüfungsbehörde vorgelegen.

Ort, Datum	Unterschrift

Belehrung

Wer vorsätzlich gegen eine die Täuschung über Prüfungsleistungen betreffende Regelung einer Hochschulprüfungsordnung verstößt, handelt ordnungswidrig. Die Ordnungswidrigkeit kann mit einer Geldbuße von bis zu 50 000 € geahndet werden. Zuständige Verwaltungsbehörde für die Verfolgung und Ahndung von Ordnungswidrigkeiten ist der Kanzler/die Kanzlerin der Technischen Universität Dortmund. Im Falle eines mehrfachen oder sonstigen schwerwiegenden Täuschungsversuches kann der Prüfling zudem exmatrikuliert werden (§ 63 Abs. 5 Hochschulgesetz –HG–).

Die Abgabe einer falschen Versicherung an Eides statt wird mit Freiheitsstrafe bis zu 3 Jahren oder mit Geldstrafe bestraft.

Die Technische Universität Dortmund wird ggf. elektronische Vergleichswerkzeuge (wie z. B. die Software "turnitin") zur Überprüfung von Ordnungswidrigkeiten in Prüfungsverfahren nutzen.

Die oben stehende Belehrung habe ich zur Kenntnis genommen.

Ort, Datum	Unterschrift